STRATEGIES FOR IMPROVING GROWTH FACTOR FUNCTION IN DIABETIC WOUNDS

By

MELISSA ANN OLEKSON

A dissertation submitted to the

Graduate School – New Brunswick

and

The Graduate School of Biomedical Sciences

University of Medicine and Dentistry of New Jersey

In partial fulfillment of the requirements

For the degree of

Doctor of Philosophy

Graduate Program in Biomedical Engineering

Written under the direction of

François Berthiaume, PhD

And approved by

_____

_____

_____

_____

_____

New Brunswick, New Jersey

October 2014

ABSTRACT OF THE DISSERTATION

Strategies for Improving Growth Factor Function in Diabetic Wounds

By MELISSA ANN OLEKSON

Dissertation Director:

François Berthiaume, PhD

Diabetic Foot Ulcers (DFUs) are debilitating non-healing wounds that often lead to amputation. The dermal scaffold is a promising treatment strategy that provides a template for cell migration and vascularization. Nevertheless, they fail in many instances due to the pro-inflammatory state of the wound, which includes increased matrix metalloproteases (MMPs) that degrade growth factors. MMPs act on both endogenous and exogenous growth factors that are added to the wound to aid in healing. Therefore, the goal of this project is to improve growth factor treatments delivered in dermal scaffolds by specifically packaging them to survive the diabetic milieu. The growth factor used here, stromal cell-derived factor-1 (SDF-1) is a chemokine that binds to the CXCR4 receptor on stem and progenitor cells; it is down-regulated in diabetes. This dissertation aims to improve SDF-1 action by blocking the pro-inflammatory receptor for advanced glycation end products (RAGE) pathway with soluble RAGE (sRAGE) and improve SDF-1 persistence using a liposome delivery system. To test the effectiveness of SDF-1, a transwell migration assay was developed, where Human Leukemia-60 (HL-60) cells, that contain the CXCR4 receptor, migrate through a porous membrane towards a supply of SDF-1. The major finding using this assay was that, as SDF-1 increases, percent cell migration increases. In addition, when HL-60 cells are pre-treated with 25mM extra glucose in cell media for 24 hours, cell migration decreased compared to cells cultured

with plain media and media supplemented with L-glucose. sRAGE treatment reversed this impairment and restored migration. The mechanism causing this phenomenon is the increased superoxide ion (O_2^-) in increased glucose cultures, which was measured through dihydroethidium. The SDF-1 liposomes were created using standard self assembly methods and also induced HL-60 cell migration in the transwell. SDF-1 liposomes maintained the induction of a calcium response associated with SDF-1 signaling. The SDF-1 liposomes also rapidly and uniformly infiltrated dermal scaffolds Alloderm® and Integra®. In an in vivo diabetic excisional wound model, sRAGE alone was not enough to restore SDF-1 function. However, SDF-1 liposomes sped up wound closure by 1 week over the controls through increased dermal cell proliferation and promotion of wound contraction.

DEDICATION

To my dear George

ACKNOWLEDGEMENTS

While this project has been the focus of my work for the past 5 years, I could not have accomplished it without the guidance and support I've received from so many mentors and friends. First, I have to thank my advisor, Dr. François Berthiaume, who has taught me so much about being a researcher and all that it entails: designing experiments, grant writing, and setting up collaborations, just to name a few. François, thank you for dedicating so much time to guiding me; I've enjoyed every day working on this project. I also want to acknowledge my committee members for all of their help. Dr. Stavroula Sofou, thank you for sharing your expertise in preparing liposomes and being generous with your laboratory supplies, equipment, and time. Dr. Ann Marie Schmidt, thank you for being an important part of this project from the start, providing expertise in diabetes biology and sRAGE for the animal experiments. I also have to thank Dr. Henry Hsia for providing clinical expertise and helping with the histology analysis and Dr. Prabhas Moghe for his continuous guidance through the development of this project.

Being in the BME department, I've had great experiences with the students, faculty and staff, in classes, the lab, and during my teaching assistantship. I want to specifically thank Dr. Rene Schloss and Dr. Martin Yarmush for being mentors throughout my undergraduate and graduate years at Rutgers and providing feedback on my work. Dr. Yarmush, thank you for the opportunity to be a part of the Biotechnology Training Program.

My labmates have been such a helpful support system over the years. Renea Faulknor, you have been such a great labmate, and, even more so, a great friend. It's been fun sharing the graduate school experience with you and you've taught me so much about experimentation and having confidence in my work. I must also thank all of the members of the Berthiaume and Yarmush labs, past and present, where each person has provided me with guidance or technical advice along the way, which I very

much appreciate! I especially want to thank Serom Lee and Andrea Gray – I have valued your friendship and support.

Outside of my lab, I have to thank everyone else who helped work on this project. Dr. Amey Bandekar and Michelle Sempkowski, thank you so much for preparing the SDF-1 liposomes and performing some of the liposome characterization. Most of all, thank you for letting me learn and observe the liposome assembly process and answering all of my questions. I have to thank Valentin Starovoytov of the Nelson Biological Laboratory Electron Imaging Facility for helping obtain the TEM images of the liposomes and Megan Anderson and Gina DiFeo of Dr. Tracey Shor's laboratory for allowing me to use their microscope to take color images of the histology slides. I acknowledge Integra LifeSciences for providing the Integra® dermal scaffolds and Luke Fritzky from the Digital Imaging and Histology Core at Rutgers-NJMS Cancer Center for his expertise in histological sectioning and staining. The veterinarians, technicians, and administrators at Lab Animal Services at Rutgers University have also been a great help in developing our animal protocols.

I have to thank Dr. Evelyn Laffey for being a mentor to me over the years and to Assistant Dean Teresa Delcorso for giving me the opportunity to be a GradFund Fellowship advisor. Teresa, not only did I further develop my own grantsmanship skills through working in your office, but I've also developed friendships with you and other fellowship advisors that will outlast my year-long position.

Last, I'm blessed with an amazing support system, and I have to thank the people who know me best: my husband, family, and friends. George, I could not have reached this point in my career without your love and support. On days when I've been discouraged, stressed, or overworked, your confidence in me has inspired my confidence in myself. Thank you for providing much needed fun on days off! My parents have also played an important role in my accomplishments. Mom and Dad, thank you for

supporting my studies and decisions up until now. You always took the time for my extracurricular science projects, whether it was raising butterflies or being a part of science league competitions. Because of you, I was able to pursue my passion, even though that involved many extra years of schooling, the sacrifice of personal time, and career opportunities that have led to a cross country move. Most importantly, you've taught me that hard work is the key to success. I have to also thank my siblings, my in-laws, and friends for their continuing support, and resisting the urge to frequently ask when I'm finishing with school. Knowing that I have you in my corner means the world to me!

TABLE OF CONTENTS

LIST OF TABLES

LIST OF ILLUSTRATIONS

1. CHAPTER 1: INTRODUCTION

1.1 ACUTE AND CHRONIC SKIN WOUNDS

Skin wounds are a growing burden on the health care system, with cost of care estimates over 20 billion dollars per year[1]. There are two major types of skin wounds: acute wounds such as burns and contusions and chronic wounds such as venous, pressure, and diabetic ulcers. While acute wounds can involve large amounts of damage and pain, they heal in a timely manner and result in a scarred, but functional skin tissue[2]. Chronic wounds, however, face an interruption in wound healing processes and fail to heal due to one or more factors: age, smoking, obesity, and underlying diseases, like diabetes[3]. Diabetic Foot Ulcers (DFUs) are a particularly devastating subset of wounds that occur in up to 6.8% of the U.S. diabetic population each year, with estimates as high as 25% of all diabetics developing a foot ulcer within their lifetime[4]. These non-healing wounds often lead to pain and infection, adversely affecting quality of life, and are subject to further complications with 82,000 amputations occurring each year[5]. The gold standard treatment for wound healing, skin grafting, usually fails in DFUs because of diabetes related impairments, such as infection and poor vascularization[6]. Many treatment strategies are being explored, with each patient receiving a customized approach based on family history, nutrition, and ulcer appearance[7]. Therefore, there is a pressing need to develop an effective treatment for all populations of DFU patients, which will only grow in number with the increase of an aging population and incidence of diabetes[8].

1.2 CURRENT DFU TREATMENTS

In a first attempt to heal a DFU, the patient's wound is provided with a moist environment, which consists of bandages, gels, and anti-inflammatory drugs[9]. If the wound remains unhealed, there are a number of more advanced techniques, which range in popularity and effectiveness: surgical debridement, vacuum assisted wound

closure (VAC), hyperbaric oxygen treatment, and the use of skin substitutes. Surgical debridement, which is very common in the clinic, is used to remove the dead tissue in the wound with a scalpel. Here, the tissue removed reveals the remaining healthy tissue underneath in an attempt to convert the wound site from chronic to acute[7]. VAC, while less common than debridement, has become popular in recent years, as the negative pressure applied can stimulate blood flow, reduce bacteria at the site, and draw the edges together. When effective, this results in a smaller or completely closed wound[10]. In patients where the wounds have low levels of oxygen, patients are sometimes placed within a hyperbaric oxygen chamber, which supplies the patient with increased atmospheric pressure and 100% oxygen. While successful in some patients, it has led to detrimental side effects, such as seizures, in others[9]. Skin substitutes, an area that has seen rapid development in the past 20 years, have also been used for both acute and chronic wounds. For the DFU afflicted population, chronic wound skin substitutes such as Dermagraft® and Apligraf® have seen average closure percentages between 50-55% in clinical trials, suggesting that there is variability in patient success and underlying diabetic pathologies can counteract the applied treatment[11, 12]. Therefore, current treatment strategies aim to correct cellular and molecular deficiencies by adding growth factors, genes, or stem cells into already FDA approved treatments[13].

1.3 DISRUPTIONS IN THE WOUND HEALING PROCESS CAUSED BY DFUs

A DFU's inability to heal is due to one or more disruptions in the multi-phase wound healing process. Traditionally, the wound healing cascade begins when a defect occurs in the skin; platelets clot the site and form a temporary fibrin matrix, resulting in a protective barrier and an initiation of the wound healing signaling cascade[14]. The next stage is inflammation, where white blood cells invade the tissue and clear out bacteria and debris during the first three days. First, neutrophils infiltrate to initially remove bacteria, and then monocytes enter, differentiate into macrophages, and further clean

the wound from debris, including engulfing spent neutrophils. This stage signals for the proliferation stage with inflammatory cytokines and growth factors[3, 15]. Over the next three weeks, fibroblasts invade, replacing the temporary matrix with secreted collagen. A provisional vascular network forms and keratinocytes proliferate and begin to close the wound edges. The final phase is remodeling, where collagen is both secreted and degraded to create the strongest, organized collagen matrix possible. This process can last from months to a year[3].

There are many factors contributing to interruptions in the wound healing process for DFUs. DFUS (as well as many other chronic wounds) are characterized by a persistence of inflammation: increased inflammatory cytokine signaling results in an influx of neutrophils and inflammatory cells at the wound site, and a subsequent increase in secreted enzymes. These enzymes, for example matrix metalloproteinases (MMPs) and elastase, degrade matrix proteins and growth factors. The degradation of exogenous growth factors has become a critical issue in potential growth factor therapies. Even when a growth factor is effective, such as the FDA-approved Regranex®, many applications are needed, which leads to complications[16, 17]. Many of these wounds remain stuck in the inflammation phase, hindering the later repair and regeneration processes[14]. Patients with diabetes also face blood flow deficiencies and hyperglycemia. Therefore, many wounds are hypoxic, leading to increased inflammation and reactive oxygen species (ROS). The hyperglycemic tissue results in increased advanced glycation end products (AGEs), which interfere with cell signaling and further enhances inflammation and ROS. This environment limits cellular activity, resulting in decreased cell motility, signaling and necessary peptides[18].

1.4 THE AGE SIGNALING PATHWAY

One pathway critical to diabetes is the signaling that the AGEs have with the receptor for AGEs (RAGE). In general, AGEs represent a large group of irreversible

products that arise when proteins are glycated in the presence of aldose sugars[19, 20]. The creation of AGEs from different sugars vary in time of production, but the hyperglycemic conditions present in diabetes increase glucose, fructose, and an overall increase in AGEs[21]. In a study by Nakamura et al., this increase in AGEs was shown to be double that of non-diabetic individuals[22]. Increased AGE levels lead to an increase in RAGE, which is a member of the immunoglobulin superfamily that has several ligands, including AGEs, S-100 proteins, and HMGB1[23]. RAGE is expressed in many different cell types, including white blood cells[23], fibroblasts[24], and keratinocytes[25], which, as described, are important for wound healing. The AGE-RAGE signaling pathway acts as a master switch in chronic inflammatory environments, as seen in figure 1.1. Activators of RAGE include high glucose (in diabetic environments), inflammatory cytokines, and RAGE ligands (like AGEs). The inflammatory activation and RAGE ligand binding stimulates intracellular generation of ROS and activation of the pro-inflammatory transcription factor, NF-κB,

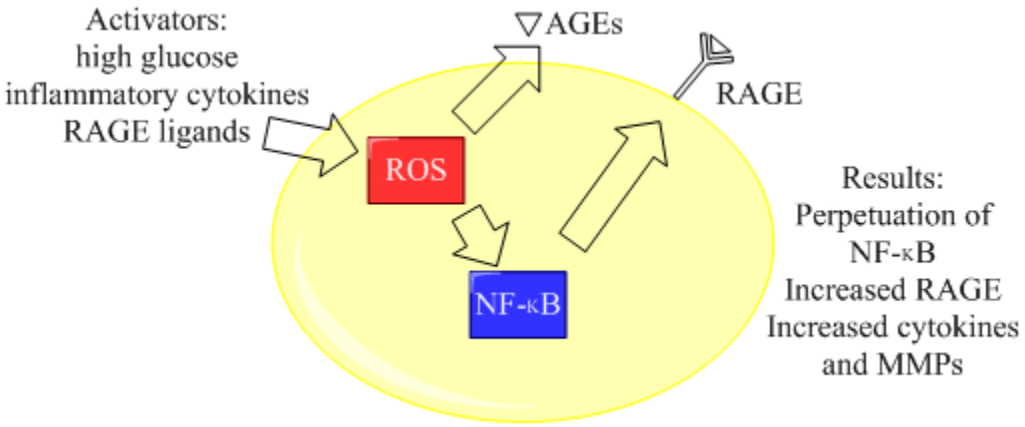

Figure 1.1 AGE-RAGE Signaling as a master switch (adapted[26]). In inflammatory environments, high glucose, inflammatory cytokines, and RAGE ligand binding stimulate the generation of ROS. This stimulation upregulates the pro-inflammatory transcription factor NF-κB, and increases the expression of RAGE. The persistent signaling results in long-term cellular dysfunction, resulting in increased NF-κB, RAGE, inflammatory cytokines, and MMPs.

which increases RAGE expression on the cell. The persistent RAGE activation induces long-term cellular dysfunction, resulting in high RAGE expression, high inflammatory cytokines, and high MMPs[26]. This dysfunction leads to functional impairments, as endothelial cells *in vitro* cultured in the presence of AGEs showed decreased migration and proliferation[19].

One possible therapeutic to decrease the inflammatory RAGE pathway is the soluble form of the RAGE receptor (sRAGE) which lacks the transmembrane domain. The sRAGE molecule is naturally produced in humans; clinical studies have shown varying results, with some studies showing diabetic patients have higher[27] or lower[28] sRAGE levels than non-diabetic patients. Therefore, the production and regulation of sRAGE is not entirely understood. In chronic environments, sRAGE has been shown to be anti-inflammatory *in vivo* and *in vitro*. When sRAGE was applied to a diabetic mouse wound healing model, the wounds closed faster, and wound analysis showed suppression of RAGE, inflammatory markers, and MMP activity[29]. The application of sRAGE to an AGE-stimulated epithelial cell culture decreased NF-κB expression and inflammatory cytokine levels[30].

1.5 STROMAL CELL-DERIVED FACTOR-1 (SDF-1)

Stromal cell-derived factor-1 (SDF-1) is the growth factor utilized in this dissertation due to its ability to attract cells, stimulate cell proliferation, and improve vascularization. SDF-1 or chemokine C-X-C- motif ligand 12 (CXCL12) is a highly positive (+9) pleiotropic molecule that binds receptors C-X-C motif G-protein coupled receptors CXCR4 and CXCR7. SDF-1 chemotaxis includes a variety of cell types, including hematopoietic stem cells, endothelial progenitor cells, and white blood cells[31, 32]. SDF-1 induces cell proliferation, as demonstrated *in vitro* through increased proliferation rates of cultured keratinocytes[33]. *In vivo*, the administration of SDF-1 induced endothelial cell migration,

enhanced survival, and upregulated vascular endothelial growth factor (VEGF), all of which led to increased vascularization in a mouse ischemic hindlimb model[32].

Through its multiple functions, SDF-1 plays an important role in wound healing. Though it is consistently present in the skin, SDF-1 is upregulated upon wounding, and elevated levels are detected on the wound margins as late as day 21 post-wounding[34]. However, in multiple models of diabetic mice, the amount of SDF-1 within wounds was shown to be decreased compared to normal mice[35, 36]. Because of this disparity, treatment with exogenous SDF-1 is a potentially attractive option for diabetic wounds. Furthermore, it may be used topically or locally as topical application of SDF-1 to wounds has been successful at improving wound healing in a normal mouse excisional acute wound model[37].

1.6 LIPOSOME DELIVERY SYSTEMS

Although SDF-1 was successful in healing wounds on normal mice, a delivery system for the SDF-1 was explored for use in diabetes because of the harsh environment accompanying DFUs that have a high concentration of MMPs. SDF-1 is sensitive to MMPs and has been shown to degrade in vitro in the presence of MMP-2 after an hour of incubation[38]. There are many biocompatible drug delivery systems available, but liposomes (self-assembled lipid vesicles) are particularly useful for wound healing studies because they can be prepared as nanosized particles, can trap drugs for delivery, and can be easily modified to enhance attributes, such as charge[39]. Liposomal delivery systems have been successfully used to deliver drugs in wound animal studies in mice and rabbits[40, 41].

1.7 WOUND HEALING ANIMAL MODELS

In vivo animal studies are included within this wounding project because, while in vitro studies are performed in highly controlled environments and evaluate a stimulus and response, they lack the cells, structure, and physiological environment found in

actual wounds. Wounds in animals can mimic the human wounds found in the clinic and provide information on the dynamic wound healing process[42]. Small rodents and pigs have typically been animals used for wound healing studies. While wound healing in pigs is most similar to human healing, they are expensive with few reagents made for pigs (e.g. antibodies), so they are not a practical first step in testing a treatment. Therefore, mouse models are widely used, with the advantages of being a low-cost, highly reproducible option[43]. Out of many wounding models available, excisional wounding, which is where a full-thickness piece of skin is removed from the dorsum, will be performed. Excisional wounding is commonly used in animal studies, though contraction is much more prominent in mice compared to humans. Even so, excisional removal of skin mimics tissue loss found in human wounds and provides an open area for easy treatment application. Wounds are evaluated for closure over time and can be histologically stained for relevant wound markers[42, 43].

1.8 DISSERTATION SUMMARY

The long range goal of this work is to improve treatment strategies for diabetic wound healing. Even the most successful of the recently developed DFU treatments, dermal scaffolds and VAC, have been limited because of the hostile DFU environment. Therefore, current projects aim at restoring balance in the wound through the use of growth factors; however, with limited success, further steps have to be taken to ensure effectiveness of growth factor treatment. The aim of this dissertation is to improve the action and persistence of exogenous SDF-1 applied in diabetic wounds. We hypothesize that SDF-1 action can be improved by the addition of sRAGE and SDF-1 persistence can be improved by liposomal packaging.

In Chapter 2, we developed a migration assay for testing the movement of Human Leukemia-60 (HL-60) cells toward SDF-1 in a transwell system. A dose response was performed and showed that, as more SDF-1 was added, the percentage

of cells migrating increased. We also show that a simulated diabetic environment (culture for 24 hours with 10-fold higher amounts of glucose than normal physiological levels) negatively impacts the migratory ability of HL-60 cells.

In Chapter 3, we tested the ability of sRAGE to improve the action of SDF-1 on the HL-60 cells. In media supplemented with high amounts of glucose, directed migration to SDF-1 was impaired. The addition of sRAGE reversed the impairment and decreased the level of intracellular AGEs. Further exploration into the mechanism revealed that high glucose culture elevated baseline ROS in the cells, which in turn, decreased the ROS spike in the SDF-1 signaling pathway. sRAGE decreased the ROS baseline and restored the SDF-1 signaling spike.

In Chapter 4, we prepared a liposomal delivery system for SDF-1. Negatively charged liposomes were combined with the positively charged peptide. The liposomes maintained a high yield of SDF-1 (around 80%) and had a uniform size distribution of 150 nm. Within the liposome packaging, the SDF-1 maintained the ability to induce directed migration and calcium signaling, as both are characteristic of free SDF-1 binding.

In Chapter 5, the developed treatments were delivered to wounds within a diabetic mouse model using FDA approved acellular dermal scaffolds. Free SDF-1 did not improve healing over the buffer control. However, sRAGE significantly improved wound healing. This closure was further improved by SDF-1 liposomes; this group showed the best healing out of all the studies. Further inspection of the SDF-1 liposome treated wounds revealed prolonged cell proliferation in the dermis of the wound, leading to faster closure.

1.9 REFERENCES

1 M. Braddock, C. J. Campbell, and D. Zuder, Current Therapies for Wound Healing: Electrical Stimulation, Biological Therapeutics, and the Potential for Gene Therapy, *Int J Dermatol,* 38 (1999), 808-17.

2 B. S. Atiyeh, J. Ioannovich, C. A. Al-Amm, and K. A. El-Musa, Management of Acute and Chronic Open Wounds: The Importance of Moist Environment in Optimal Wound Healing, *Curr Pharm Biotechnol,* 3 (2002), 179-95.

3 C. Harvey, Wound Healing, *Orthopedic Nursing,* 24 (2005), 143-59.

4 I. Chow, E. V. Lemos, and T. R. Einarson, Management and Prevention of Diabetic Foot Ulcers and Infections: A Health Economic Review, *Pharmacoeconomics,* 26 (2008), 1019-35.

5 J Jean, M Estrella Garcia-Pérez, and R Pouliot, Bioengineered Skin: The Self-Assembly Approach, *Tissue Science & Engineering,* 5 (2011), 1-10.

6 L. Macri, and R. A. Clark, Tissue Engineering for Cutaneous Wounds: Selecting the Proper Time and Space for Growth Factors, Cells and the Extracellular Matrix, *Skin Pharmacol Physiol,* 22 (2009), 83-93.

7 M. A. Fonder, G. S. Lazarus, D. A. Cowan, B. Aronson-Cook, A. R. Kohli, and A. J. Mamelak, Treating the Chronic Wound: A Practical Approach to the Care of Nonhealing Wounds and Wound Care Dressings, *J Am Acad Dermatol,* 58 (2008), 185-206.

8 N. S. Greaves, S. A. Iqbal, M. Baguneid, and A. Bayat, The Role of Skin Substitutes in the Management of Chronic Cutaneous Wounds, *Wound Repair Regen,* 21 (2013), 194-210.

9 S. Enoch, J. E. Grey, and K. G. Harding, Abc of Wound Healing. Non-Surgical and Drug Treatments, *BMJ,* 332 (2006), 900-3.

10 G. Preston, An Overview of Topical Negative Pressure Therapy in Wound Care, *Nurs Stand,* 23 (2008), 62-4, 66, 68.

11 W. A. Marston, Dermagraft, a Bioengineered Human Dermal Equivalent for the Treatment of Chronic Nonhealing Diabetic Foot Ulcer, *Expert Rev Med Devices,* 1 (2004), 21-31.

12 A. Veves, V. Falanga, D. G. Armstrong, and M. L. Sabolinski, Graftskin, a Human Skin Equivalent, Is Effective in the Management of Noninfected Neuropathic Diabetic Foot Ulcers: A Prospective Randomized Multicenter Clinical Trial, *Diabetes Care,* 24 (2001), 290-5.

13 C. I. Gunter, and H. G. Machens, New Strategies in Clinical Care of Skin Wound Healing, *Eur Surg Res,* 49 (2012), 16-23.

14 R. F. Diegelmann, and M. C. Evans, Wound Healing: An Overview of Acute, Fibrotic and Delayed Healing, *Front Biosci,* 9 (2004), 283-9.

15 T. J. Shaw, and P. Martin, Wound Repair at a Glance, *J Cell Sci,* 122 (2009), 3209-13.

16 Schultz GS Chin GA, Chegini N, Diegelmann RF, 'Biochemistry of Wound Healing in Wound Care Practice', in *Wound Care Practice*, ed. by Paul SheffieldBest Publishing, Co., 2007).

17 R. C. Fang, and R. D. Galiano, A Review of Becaplermin Gel in the Treatment of Diabetic Neuropathic Foot Ulcers, *Biologics,* 2 (2008), 1-12.

18 S. Guo, and L. A. Dipietro, Factors Affecting Wound Healing, *J Dent Res,* 89 (2010), 219-29.

19 Q. Chen, L. Dong, L. Wang, L. Kang, and B. Xu, Advanced Glycation End Products Impair Function of Late Endothelial Progenitor Cells through Effects on

Protein Kinase Akt and Cyclooxygenase-2, *Biochem Biophys Res Commun,* 381 (2009), 192-7.

20 M. Takeuchi, and S. Yamagishi, Possible Involvement of Advanced Glycation End-Products (Ages) in the Pathogenesis of Alzheimer's Disease, *Curr Pharm Des,* 14 (2008), 973-8.

21 N. Ahmed, Advanced Glycation Endproducts--Role in Pathology of Diabetic Complications, *Diabetes Res Clin Pract,* 67 (2005), 3-21.

22 K. Nakamura, S. Yamagishi, H. Adachi, Y. Kurita-Nakamura, T. Matsui, T. Yoshida, and T. Imaizumi, Serum Levels of Srage, the Soluble Form of Receptor for Advanced Glycation End Products, Are Associated with Inflammatory Markers in Patients with Type 2 Diabetes, *Mol Med,* 13 (2007), 185-9.

23 R. Clynes, B. Moser, S. F. Yan, R. Ramasamy, K. Herold, and A. M. Schmidt, Receptor for Age (Rage): Weaving Tangled Webs within the Inflammatory Response, *Curr Mol Med,* 7 (2007), 743-51.

24 C. Schlueter, S. Hauke, A. M. Flohr, P. Rogalla, and J. Bullerdiek, Tissue-Specific Expression Patterns of the Rage Receptor and Its Soluble Forms--a Result of Regulated Alternative Splicing?, *Biochim Biophys Acta,* 1630 (2003), 1-6.

25 P. Zhu, M. Ren, C. Yang, Y. X. Hu, J. M. Ran, and L. Yan, Involvement of Rage, Mapk and Nf-Kappab Pathways in Ages-Induced Mmp-9 Activation in Hacat Keratinocytes, *Exp Dermatol,* 21 (2012), 123-9.

26 A. Bierhaus, P. M. Humpert, D. M. Stern, B. Arnold, and P. P. Nawroth, Advanced Glycation End Product Receptor-Mediated Cellular Dysfunction, *Ann N Y Acad Sci,* 1043 (2005), 676-80.

27 Y. M. Arabi, M. Dehbi, A. H. Rishu, E. Baturcam, S. H. Kahoul, R. J. Brits, B. Naidu, and A. Bouchama, Srage in Diabetic and Non-Diabetic Critically Ill Patients: Effects of Intensive Insulin Therapy, *Crit Care,* 15 (2011), R203.

28 X. D. Su, S. S. Li, Y. Q. Tian, Z. Y. Zhang, G. Z. Zhang, and L. X. Wang, Elevated Serum Levels of Advanced Glycation End Products and Their Monocyte Receptors in Patients with Type 2 Diabetes, *Arch Med Res,* 42 (2011), 596-601.

29 M. T. Goova, J. Li, T. Kislinger, W. Qu, Y. Lu, L. G. Bucciarelli, S. Nowygrod, B. M. Wolf, X. Caliste, S. F. Yan, D. M. Stern, and A. M. Schmidt, Blockade of Receptor for Advanced Glycation End-Products Restores Effective Wound Healing in Diabetic Mice, *Am J Pathol,* 159 (2001), 513-25.

30 M. Morcos, A. A. Sayed, A. Bierhaus, B. Yard, R. Waldherr, W. Merz, I. Kloeting, E. Schleicher, S. Mentz, R. F. Abd el Baki, H. Tritschler, M. Kasper, V. Schwenger, A. Hamann, K. A. Dugi, A. M. Schmidt, D. Stern, R. Ziegler, H. U. Haering, M. Andrassy, F. van der Woude, and P. P. Nawroth, Activation of Tubular Epithelial Cells in Diabetic Nephropathy, *Diabetes,* 51 (2002), 3532-44.

31 A. Dar, P. Goichberg, V. Shinder, A. Kalinkovich, O. Kollet, N. Netzer, R. Margalit, M. Zsak, A. Nagler, I. Hardan, I. Resnick, A. Rot, and T. Lapidot, Chemokine Receptor Cxcr4-Dependent Internalization and Resecretion of Functional Chemokine Sdf-1 by Bone Marrow Endothelial and Stromal Cells, *Nat Immunol,* 6 (2005), 1038-46.

32 J. Yamaguchi, K. F. Kusano, O. Masuo, A. Kawamoto, M. Silver, S. Murasawa, M. Bosch-Marce, H. Masuda, D. W. Losordo, J. M. Isner, and T. Asahara, Stromal Cell-Derived Factor-1 Effects on Ex Vivo Expanded Endothelial Progenitor Cell Recruitment for Ischemic Neovascularization, *Circulation,* 107 (2003), 1322-8.

33 L. Florin, N. Maas-Szabowski, S. Werner, A. Szabowski, and P. Angel, Increased Keratinocyte Proliferation by Jun-Dependent Expression of Ptn and Sdf-1 in Fibroblasts, *J Cell Sci,* 118 (2005), 1981-9.

34 A. Toksoy, V. Muller, R. Gillitzer, and M. Goebeler, Biphasic Expression of Stromal Cell-Derived Factor-1 During Human Wound Healing, *Br J Dermatol,* 157 (2007), 1148-54.

35 K. A. Gallagher, Z. J. Liu, M. Xiao, H. Chen, L. J. Goldstein, D. G. Buerk, A. Nedeau, S. R. Thom, and O. C. Velazquez, Diabetic Impairments in No-Mediated Endothelial Progenitor Cell Mobilization and Homing Are Reversed by Hyperoxia and Sdf-1 Alpha, *J Clin Invest,* 117 (2007), 1249-59.

36 T. E. Restivo, K. A. Mace, A. H. Harken, and D. M. Young, Application of the Chemokine Cxcl12 Expression Plasmid Restores Wound Healing to near Normal in a Diabetic Mouse Model, *J Trauma,* 69 (2010), 392-8.

37 A. Sarkar, S. Tatlidede, S. S. Scherer, D. P. Orgill, and F. Berthiaume, Combination of Stromal Cell-Derived Factor-1 and Collagen-Glycosaminoglycan Scaffold Delays Contraction and Accelerates Reepithelialization of Dermal Wounds in Wild-Type Mice, *Wound Repair Regen,* 19 (2011), 71-9.

38 H. Peng, Y. Wu, Z. Duan, P. Ciborowski, and J. C. Zheng, Proteolytic Processing of Sdf-1alpha by Matrix Metalloproteinase-2 Impairs Cxcr4 Signaling and Reduces Neural Progenitor Cell Migration, *Protein Cell,* 3 (2012), 875-82.

39 M. B. R. Pierre, and I. D. M. Costa, Liposomal Systems as Drug Delivery Vehicles for Dermal and Transdermal Applications, *Archives of Dermatological Research,* 303 (2011), 607-21.

40 F. Roesken, E. Uhl, S. B. Curri, M. D. Menger, and K. Messmer, Acceleration of Wound Healing by Topical Drug Delivery Via Liposomes, *Langenbecks Arch Surg,* 385 (2000), 42-9.

41 J. Wang, R. Wan, Y. Mo, M. Li, Q. Zhang, and S. Chien, Intracellular Delivery of Adenosine Triphosphate Enhanced Healing Process in Full-Thickness Skin Wounds in Diabetic Rabbits, *Am J Surg,* 199 (2010), 823-32.

42 F. Gottrup, M. S. Agren, and T. Karlsmark, Models for Use in Wound Healing Research: A Survey Focusing on in Vitro and in Vivo Adult Soft Tissue, *Wound Repair Regen,* 8 (2000), 83-96.

43 V. W. Wong, M. Sorkin, J. P. Glotzbach, M. T. Longaker, and G. C. Gurtner, Surgical Approaches to Create Murine Models of Human Wound Healing, *J Biomed Biotechnol,* 2011 (2011), 969618.

2. CHAPTER 2: DEVELOPMENT OF AN IN VITRO TRANSWELL MIGRATION SYSTEM TO EVALUATE SDF-1 DIRECTED MIGRATION OF HL-60 CELLS

2.1 INTRODUCTION

Being a pleiotropic chemokine, SDF-1 induces multiple cell types to migrate towards a source; it also stimulates cell proliferation and survival. Upon binding to its G-protein coupled receptor, CXCR4, a portion of the signaling cascade activates phosphoinositide 3-kinase (PI3K), which stimulates various responses, including motility signals, such as focal adhesion kinase (FAK)[1, 2]. Because of SDF-1's importance in the context of wound healing, characterizing the ability of SDF-1 to stimulate migration in simulated chronic conditions, such as diabetes, requires use of an *in vitro* migration assay. Using *in vitro* migration assays to complement the *in vivo* experiments allows for highly reproducible, high throughput experiments that can confirm a phenomenon prior to use in animals[3]. The hypothesis is that an in vitro transwell migration assay can show SDF-1 directed migration, and that a simulated diabetic environment (high glucose culture) can impact this migration.

Out of the many *in vitro* migration assays available, the transwell assay, traditionally known as a Boyden chamber, is one of the most commonly used setups. As

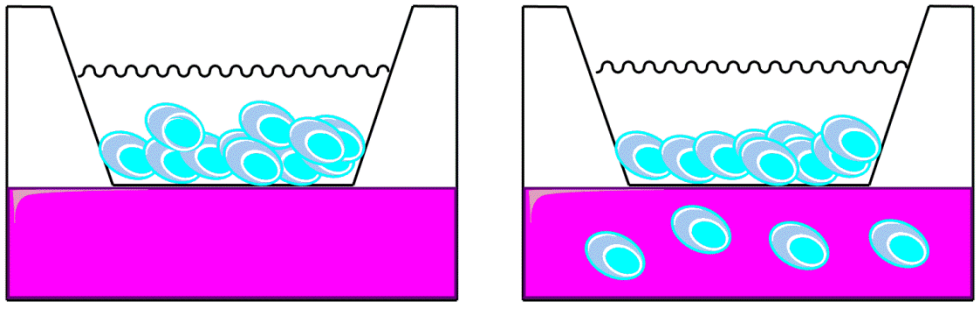

Figure 2.1 Transwell Migration Assay. The cells are placed in the upper compartment at the start (left) and allowed to migrate through the membrane over time to the bottom compartment (right).

seen in figure 2.1, the transwell assay has an upper compartment and a lower compartment separated by a porous membrane. The cells are placed above the membrane (where the pore diameter is less than the cell diameter) and the chemotactic cue is placed below the membrane. Over time, the cells migrate through the membrane and can be collected and analyzed. The direction and speed of cell migration can easily be determined using a transwell migration assay, which makes it favorable even though the gradient can only be sustained over a short duration[4].

Though transwell assays are commonly used, parameters vary based on cell type and chemotactic cue. Our studies utilize Human Leukemia-60 (HL-60) cells, a pro-myelocytic cell line, which highly express the SDF-1 receptor CXCR4[5]. Because of this expression, a migration response occurs in HL-60s upon SDF-1 binding. The round quiescent HL-60 morphology changes in a matter of seconds upon SDF-1 binding, whereby actin filaments within the cells polymerize causing blebs in the cell membrane and migration in a matter of minutes[6]. In a study by Carrigan et al., HL-60 cells were used in a transwell and migrated over the course of 70 minutes[7].

We established a transwell assay to measure directed SDF-1 migration of HL-60 cells. To simulate the diabetic environment found *in vivo*, high glucose was added to cell media prior to migration. Supplementation of 12-30 mM glucose has been shown to inhibit cellular migration compared to control media[8, 9]. Through these studies, we determined transwell parameters, usable SDF-1 doses, and glucose concentrations to use in this project.

2.2 METHODS

2.2.1 Cell Culture

HL-60 cells were purchased from American Type Culture Collection (ATCC). Cultures were maintained in T-75 flasks (Becton, Dickinson) at 10^5 - 10^6 cells/mL in

Iscove's Modified Dulbecco's Medium (IMDM) supplemented with 20% Fetal Bovine Serum (FBS) and penicillin-streptomycin (Life Technologies).

2.2.2 Transwell Migration Assay

HL-60 cells were suspended at 10^6 cells/mL in IMDM and a total of 10^5 cells in 100μL medium were placed on top of a 24-well plate transwell porous insert (transparent polyethylene terephthalate (PET) membrane, 8μm pores, Corning). The bottom of the well was preloaded with 600μL of IMDM or IMDM supplemented with 25, 50, 100, or 200 ng/mL SDF-1 (R&D systems). Plates were incubated at 37°C and harvested after 70 minutes. The number of cells that passed through to the bottom well were counted using a hemacytometer (Hausser) and normalized to the initial number of added cells (10^5 cells).

2.2.3 Dextran Tracer Measurements

A fluorescent tracer was used to measure the gradient within the transwell after 70 minutes. A 10,000 Da fluoresein isothiocyante (FITC)-dextran (Sigma-Aldrich) was suspended at a concentration of 100ng/mL in Phosphate Buffered Saline (PBS, OmniPur). This particular size was chosen because it is fairly similar to the molecular weight of SDF-1 (8000 Da), and therefore assumed to diffuse at a similar rate. Fluorescent images were taken of wells containing 100 ng/mL dextran and PBS control. Images were then taken of the transwell PET membrane placed in the FITC-dextran well every 5 minutes for 70 minutes. Mean Fluorescence Intensity (MFI) was assessed using the ImageJ software (NIH).

2.2.4 High Glucose Cell Culture

For select migration studies, cells were first cultured with high glucose supplemented media to simulate a diabetic environment. Cells were transferred from flask culture to 12-well plates (Becton, Dickinson) at 500,000 cells/mL in full IMDM

media that had 12.5, 25, and 50 mM added D-glucose (Sigma Aldrich). Cells were cultured for 24 hours prior to testing in the transwell migration assay. All culture levels of glucose are approximations of diabetes-relevant conditions, compared to non-diabetic clinical levels of 5 mM[10]. The 10-fold increase in glucose levels compared to the normal levels, while appropriate for the model cell culture system, would not be compatible on a persistent basis with life.

2.2.5 Statistics

All values are presented as means ± standard error of the mean (SEM). Multiple comparisons were carried out using one-way ANOVA followed by post-hoc analysis. Post-hoc tests are indicated in the figure legends.

2.3 RESULTS AND DISCUSSION

2.3.1. SDF-1 Directed Migration of HL-60 cells

A dose response of SDF-1 was administered in the transwell to determine migration ability of HL-60 cells (figure 2.2). Starting at 50 ng/mL SDF-1, there was a significant response of HL-60 migration compared to the control (basal media). While 200ng/mL elicited the greatest response, this experiment confirmed that a commonly used dose of SDF-1 concentration to stimulate chemotaxis (100ng/mL)[11] would also be effective in our studies. Therefore, future studies will utilize this SDF-1 dose.

2.3.2. Dextran Tracer to Mock SDF-1 in Transwells

To complement the dose response findings, FITC-dextran tracer measurements were performed, where the FITC-dextran mimics SDF-1. First, the membrane of the transwell was fluorescently imaged at the start (time = 0 minutes) and end (time = 70 minutes) of the migration experiment (figure 3A). The membrane at time = 70 minutes was bright green (the color of the FITC-Dextran), showing that the FITC dextran had reached the transwell membrane after being placed at the bottom. We then compared

fluorescent images of the membrane to those of the initial fluorescence of the dextran. The initial mean fluorescence intensity (MFI) of the dextran and PBS were 5100 and 3900 a.u., respectively. At time = 0 minutes, the addition of the dextran to the bottom of the transwell increased the fluorescence intensity to 4700 a.u., which then reached 5000 a.u. after 20 minutes of incubation. Therefore, the dextran, and, subsequently, the SDF-1, reaches the membrane over the duration of the transwell migration.

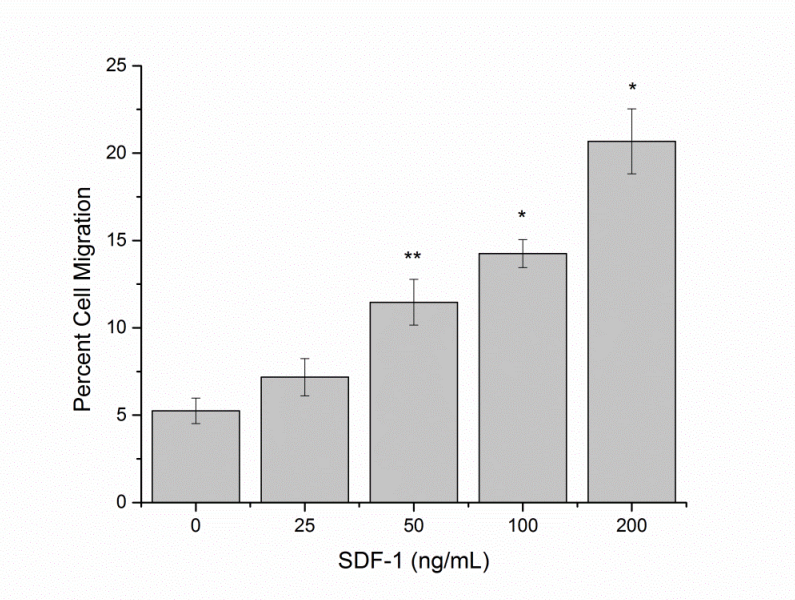

Figure 2.2 SDF-1 Dose Response of HL-60 Migration. HL-60 cells (10^5 in 100µL) were placed on top of a transwell in a 24-well plate. The bottom of the well was filled with 600µL of basal IMDM media or media containing 25, 50, 100, or 200 ng/mL SDF-1. Data shown are the number of cells that migrated across the membrane after 70 minutes normalized to the number of cells added to the well. N=7. (*: p < 0.01, **: p < 0.05, one way ANOVA, Fisher's LSD post-test).

2.3.3. Migration of HL-60 cells After High Glucose Culture

We then compared the SDF-1 directed HL-60 migration to HL-60 migration in the presence of added glucose (figure 2.4). Compared to basal media, the addition of glucose decreased HL-60 cell migration as glucose concentration increased. Significant levels of decreased migration were observed at 25mM and 50mM added glucose.

2.4 CONCLUSION

The purpose of this chapter was to develop a migration assay and simulated diabetic environment to test the effect of SDF-1 and sRAGE treatment in high glucose. In the developed transwell assay, as SDF-1 increased higher than 50 ng/mL, cell migration increased significantly compared to the control. We utilized a fluorescent dextran tracer similar in size to SDF-1 to confirm that the transwell setup we use allows the dextran, and in turn, SDF-1, to diffuse through the membrane where the cells can bind SDF-1 and begin the migration signaling cascade. When we cultured cells in a simulated diabetic environment of full cell culture media supplemented with additional glucose, the HL-60 cell migration decreased, showing that the additional glucose impacts directed migration to SDF-1. Future studies will utilize the transwell parameters, as well as dose of SDF-1 (100ng/mL) and added concentration of glucose (25mM) to further understand the mechanisms of SDF-1 in the diabetic environment.

A

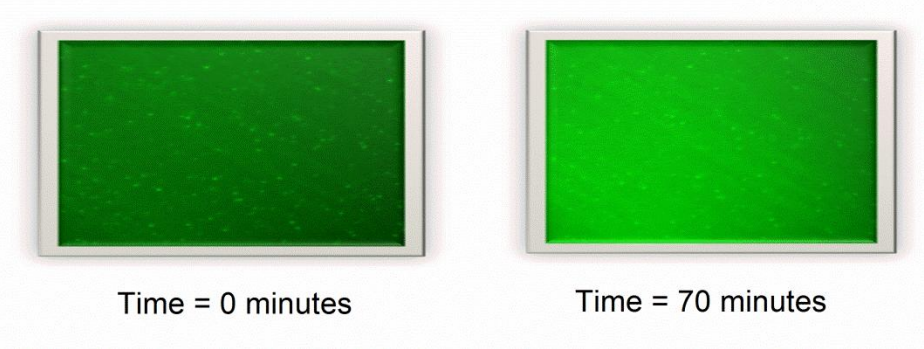

B

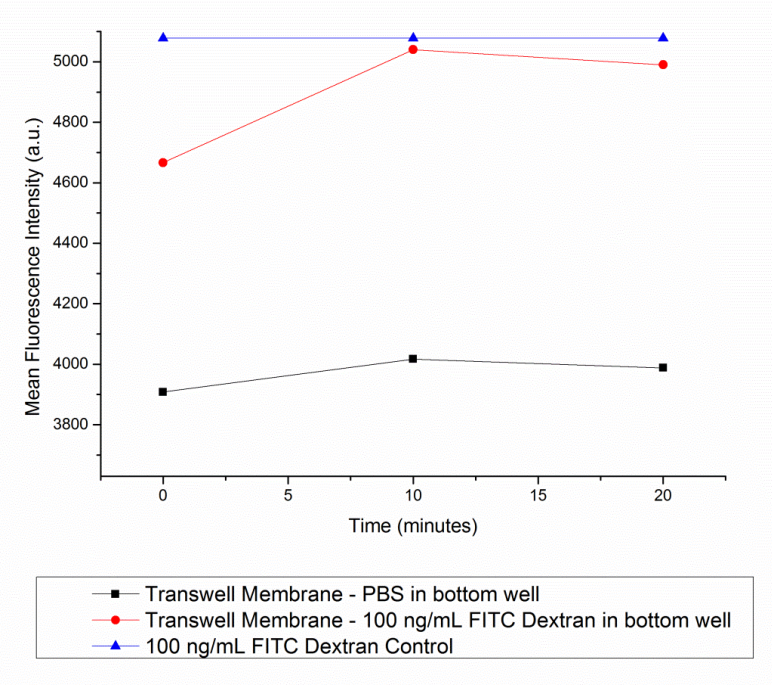

Figure 2.3 Dextran Tracer Measurements. (A) 600µL of 100ng/mL of FITC-Dextran in PBS was placed in the bottom of a 24-well transwell. Fluorescent images of the membrane were taken at time = 0 minutes (left) and time = 70 minutes (right) after the dextran was added. (B) Mean Fluorescent Intensity of PBS (square) and FITC dextran (triangle) were determined by fluorescent imaging. After the transwell insert was placed in the FITC-dextran well, images of the membrane were taken every 5 minutes, reaching the level of the control FITC-dextran by 20 minutes.

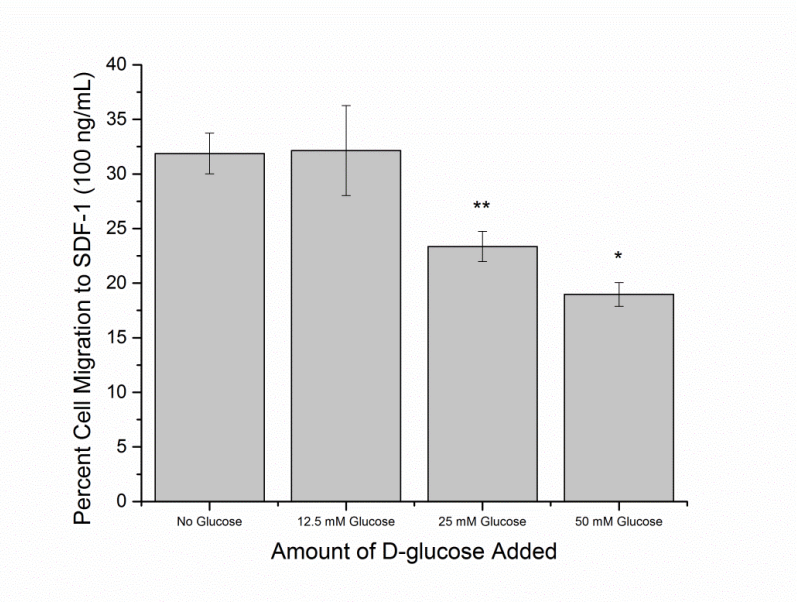

Figure 2.4 Influence of Glucose on SDF-1 Directed Migration. HL-60 cells (10^5 in 100µL) were placed on top of a transwell in a 24-well plate after 24 hour culture with 12.5, 25, or 50 mM added glucose. After culture, the cells were resuspended in fresh IMDM media without added glucose. The bottom of the well was filled with 600µL of basal IMDM media or media containing 100 ng/mL SDF-1. Data shown are the number of cells that migrated across the membrane after 70 minutes normalized to the number of cells added to the well. N=7. (*: $p < 0.01$, **: $p < 0.05$, one way ANOVA, Fisher's LSD post-test).

2.5 REFERENCES

1 F. Barbieri, A. Bajetto, and T. Florio, Role of Chemokine Network in the Development and Progression of Ovarian Cancer: A Potential Novel Pharmacological Target, *J Oncol,* 2010 (2010), 426956.

2 W. T. Choi, S. Duggineni, Y. Xu, Z. Huang, and J. An, Drug Discovery Research Targeting the Cxc Chemokine Receptor 4 (Cxcr4), *J Med Chem,* 55 (2012), 977-94.

3 N. Kramer, A. Walzl, C. Unger, M. Rosner, G. Krupitza, M. Hengstschlager, and H. Dolznig, In Vitro Cell Migration and Invasion Assays, *Mutat Res,* 752 (2013), 10-24.

4 S. Toetsch, P. Olwell, A. Prina-Mello, and Y. Volkov, The Evolution of Chemotaxis Assays from Static Models to Physiologically Relevant Platforms, *Integr Biol (Camb),* 1 (2009), 170-81.

5 C. Bogani, V. Ponziani, P. Guglielmelli, C. Desterke, V. Rosti, A. Bosi, M. C. Le Bousse-Kerdiles, G. Barosi, and A. M. Vannucchi, Hypermethylation of Cxcr4 Promoter in Cd34+ Cells from Patients with Primary Myelofibrosis, *Stem Cells,* 26 (2008), 1920-30.

6 C. Voermans, E. C. Anthony, E. Mul, E. van der Schoot, and P. Hordijk, Sdf-1-Induced Actin Polymerization and Migration in Human Hematopoietic Progenitor Cells, *Exp Hematol,* 29 (2001), 1456-64.

7 S. O. Carrigan, A. L. Weppler, A. C. Issekutz, and A. W. Stadnyk, Neutrophil Differentiated Hl-60 Cells Model Mac-1 (Cd11b/Cd18)-Independent Neutrophil Transepithelial Migration, *Immunology,* 115 (2005), 108-17.

8 C. C. Lan, I. H. Liu, A. H. Fang, C. H. Wen, and C. S. Wu, Hyperglycaemic Conditions Decrease Cultured Keratinocyte Mobility: Implications for Impaired Wound Healing in Patients with Diabetes, *Br J Dermatol,* 159 (2008), 1103-15.

9 T. Wuensch, F. Thilo, K. Krueger, A. Scholze, M. Ristow, and M. Tepel, High Glucose-Induced Oxidative Stress Increases Transient Receptor Potential Channel Expression in Human Monocytes, *Diabetes,* 59 (2010), 844-9.

10 B. Vasarhelyi, P. Bencsik, A. Treszl, Z. Bardoczy, T. Tulassay, and M. Szathmari, The Effect of Physiologic Hyperinsulinemia During an Oral Glucose Tolerance Test on the Levels of Dehydroepiandrosterone (Dhea) and Its Sulfate (Dheas) in Healthy Young Adults Born with Low and with Normal Birth Weight, *Endocr J,* 50 (2003), 689-95.

11 A. Aiuti, I. J. Webb, C. Bleul, T. Springer, and J. C. Gutierrez-Ramos, The Chemokine Sdf-1 Is a Chemoattractant for Human Cd34+ Hematopoietic Progenitor Cells and Provides a New Mechanism to Explain the Mobilization of Cd34+ Progenitors to Peripheral Blood, *J Exp Med,* 185 (1997), 111-20.

3. CHAPTER 3: BLOCKING RAGE REVERSES SDF-1 FUNCTION IMPAIRMENT INDUCED BY SIMULATED DIABETES CELL CULTURE

3.1 INTRODUCTION

Through an *in vitro* transwell migration assay, we observed that SDF-1 directed migration of HL-60 cells decreases in the presence of media with extra glucose added. This impairment is consistent with the decreased action of SDF-1 in simulated diabetic environments in the literature[1]. To improve the simulated diabetic environment, soluble RAGE (sRAGE), a form of the RAGE receptor that lacks the transmembrane domain, is used as an anti-inflammatory RAGE blocking agent[2]. The hypothesis is that the migratory function of HL-60 cells to SDF-1 will be restored upon attenuation of the inflammatory diabetic environment by using sRAGE. It is also expected that the amount of AGEs and ROS produced will decrease with sRAGE treatment.

SDF-1 production and action has previously been shown to be affected by diabetes *in vivo* and *in vitro*. In wounds created in both streptozotocin induced and genetically diabetic mice, SDF-1 levels were decreased post-wounding compared to normal mice[3, 4]. In addition to lower production, simulated diabetic cell cultures also show decreased cell migration. In a study by Li et al., endothelial progenitor cells cultured in a high AGE environment produced less SDF-1 and migrated less than normal cultured cells[1]. There are deficiencies in SDF-1 that can be further explored in pro-inflammatory, diabetic environments.

To combat the pro-inflammatory environment, sRAGE has been used to block the RAGE pathway and associated inflammation. In genetically diabetic mouse wounds, the addition of sRAGE not only accelerates healing, but also decreases RAGE expression and the production of tumor necrosis factor alpha (TNFα), interleukin-6 (IL-6), and MMPs[2]. *In vitro*, kidney proximal tubular epithelial cells (pTECs) were cultured in the presence of AGEs. The addition of sRAGE decreased the expression of NF-KB and

the production of IL-6, compared to controls[5]. While sRAGE has been shown to decrease RAGE and attenuate the pro-inflammatory environment, the anti-inflammatory mechanisms and effects on growth factors need to be further elucidated.

To understand the interaction between SDF-1 and AGEs, it is important to understand the signaling cascades associated with each molecule. Upon SDF-1 binding of the CXCR4 receptor, two parallel signaling cascades are activated. Binding induces phospholipase C (PLC), in turn producing the secondary messenger inositol triphosphate (IP3), releasing Ca^{2+} into the cell from the endoplasmic reticulum. The calcium release and direct binding activate extracellular signal-regulated kinase (ERK) 1 and 2, resulting in cell proliferation. Alternatively, binding induces a transient production of ROS and the activation of phosphoinositide 3 kinase (PI3K) to induce cell migration and survival[6, 7]. Cells in culture have been observed to increase intracellular ROS within seconds when incubated with SDF-1[8]. Using sRAGE as a therapeutic blocks the AGE activated RAGE signaling pathway, which is chronically pro-inflammatory, increasing the expression of NF-κB, pro-inflammatory cytokines, and inflammation[9]. In addition, the activation of RAGE increases levels of ROS in the cell[10] and signals mDia1, an intracellular signaling partner to RAGE, which has been implicated in smooth muscle cell migration and expansion[11].

Therefore, while the signaling cascades of SDF-1 and AGEs do not directly interact, they both affect ROS levels, which are known to impact cell migration. It is clear that ROS is necessary for migration; when NADPH oxidase, the enzyme used to create superoxide, is blocked in neutrophils, they experience decreased migration[12]. However, excess levels of ROS are also detrimental. In a study by van Aalst et al., incubation of endothelial cells with oxidized low-density lipoprotein (LDL) both increased ROS levels and decreased cell migration compared to cells cultured in normal media[13]. Studies presented here further investigate the interaction of pro-inflammatory, high ROS

environments on SDF-1 directed migration in a simulated diabetic environment. The blocking molecule sRAGE is utilized as an anti-inflammatory molecule to improve the action of SDF-1.

3.2 METHODS

3.2.1 Cell Culture

HL-60 cells were purchased from American Type Culture Collection (ATCC). Cultures were maintained in T-75 flasks (Becton, Dickinson) at 10^5 - 10^6 cells/mL in Iscove's Modified Dulbecco's Medium (IMDM) supplemented with 20% Fetal Bovine Serum (FBS) and penicillin-streptomycin (Life Technologies).

3.2.2 Transwell Migration Assay

HL-60 cells were suspended at 10^6 cells/mL in IMDM and a total of 10^5 cells in 100μL medium were placed on top of a 24-well plate transwell porous insert (transparent polyethylene terephthalate (PET) membrane, 8μm pores, Corning). The bottom of the well was preloaded with 600μL of IMDM or IMDM supplemented with 100ng/mL SDF-1 (R&D systems), 500ng/mL sRAGE (Adipo Bioscience), or 100ng/mL SDF-1 and 500ng/mL sRAGE. Plates were incubated at 37°C and harvested after 70 minutes. The number of cells that passed through to the bottom well were counted using a hemacytometer (Hausser) and normalized to the initial number of added cells (10^5 cells).

3.2.3 High Glucose Cell Culture

For select migration studies, cells were first cultured with high glucose supplemented media to simulate a diabetic environment. Cells were transferred from flask culture to 12-well plates (Becton, Dickinson) at 500,000 cells/mL in full IMDM media that had 25 mM added D-glucose (Sigma Aldrich). Control cultures had media supplemented with the glucose enantiomer L-glucose (Sigma Aldrich), a commonly used control that is not metabolized by the cells[14]. Cells were cultured for 24 hours prior to

testing in the transwell migration assay. Additional experiments had added 500 ng/mL sRAGE into the 24 media with D-glucose culture.

3.2.4 HL-60 Viability

To test for viability, HL-60 cells were suspended in phosphate buffered saline (PBS, OmniPur) at 2 x 10^6 cells/mL. 10 μL of cells was placed in a small sterile Petri dish and 150 μL of stain solution (2μM carboxyfluoroscein diacetate and 4μM propidium iodide, MarkerGene Technologies) was placed over the droplet of cell suspension. After 30 minutes of incubation at 37°C, the cells were imaged under an Olympus IX81® microscope to visualize live cells (green) and dead cells (red). Three images were taken for each replicate and percent viability was calculated as number of live (green) cells/total cells (red+green) x 100. Fluorescent cells were compared with brightfield images to ensure cell count was accurate.

3.2.5 Flow Cytometry

HL-60 cells were analyzed for CXCR4 receptor expression. First, cells were washed three times with PBS + 0.1% Bovine Serum Albumin (BSA, Sigma Aldrich). After washing, the cells were resuspended at 4 x 10^6 cells/mL in PBS. 100,000 cells of each condition were blocked with 2 μL mouse serum (Life Technologies) and incubated with 10 μL of antibody (either mouse IgG2A isotype control-allophycocyanin (APC) or mouse monoclonal anti-human CXCR4-APC, R&D Systems) for 40 minutes at 4°C. The cells were washed two times in PBS and resuspended in 200 μL PBS. 10,000 cells from each condition were run on a FACSCalibur 2 laser flow cytometer (BD Biosciences) for APC fluorescence (FL-4). CellQuest (Becton, Dickinson) software was used to acquire and analyze the results. Flourescence was gated at 5%.

3.2.6 Mononuclear Cell Isolation and Migration

Primary mononuclear white blood cells were isolated from the blood of C57BL/6 mice (Charles River) and diabetic Lepr^{db} modified black mice (Jackson Laboratory). Briefly, mice were anesthetized using isofluorane (Henry Schein), and sufficiently under anesthesia when there is no contraction reflex with a toe pinch. The mouse is held by the scruff of the skin by the shoulders and a 22-gauge needle is inserted 5-mm from the center of the thorax towards the chin at a 25° angle. The blood is collected into tubes with sodium citrate, an anti-coagulant (Sigma-Aldrich). The blood then undergoes gradient separation using Ficoll-paque. Every 2 mL of blood is mixed with 2 mL of Roswell Park Memorial Institute (RPMI) media (Life Technologies). The 4 mL are then carefully pipetted onto 3 mL of Ficoll-paque Premium 1.084 (GE Lifesciences). After 60 minutes of centrifugation at 400 x g, the plasma layer is removed and the mononuclear cell layer is washed before use in the migration assay.

3.2.7 AGE Immunocytochemistry

After 24 hour culture with or without glucose, cells were resuspended to 50,000 cells/mL in PBS and 1 mL (50,000 cells) was placed in each well of a 24-well plate. Cells were spun in centrifuge in the plates for 2 minutes at 1000 rpm to settle the cells to the bottom of the plate. The cells were washed and incubated for 15 minutes at room temperature with a 4% paraformaldehyde solution (Sigma Aldrich). Cells were washed three times with PBS and were incubated with a solution of 10% goat serum (Life Technologies) and 0.1% triton-x (Sigma Aldrich) in PBS for 45 minutes at room temperature. Cells were incubated with primary antibody (rabbit polyclonal anti-AGE (R&D systems) or Rabbit IgG Isotype Contrl (Millipore)) at 5 µg/mL overnight at 4°C. The following day, cells were brought to room temperature, washed three times with PBS and incubated with the secondary antibody goat anti-rabbit IgG fluorescein (R&D systems) for 1 hour at 1.25 µg/mL. The cells were washed twice with PBS, counterstained with 4', 6-Diamino-2-phenylindole dihydrochloride (DAPI) (1:5000, Life

Technologies) for 10 minutes and washed again. The cells were imaged using under an Olympus IX81® microscope to visualize positively stained cells (green) and number of cells (blue). Five images were taken for each replicate and fluorescence per cell was determined using ImageJ software (NIH) after subtraction of background. Mean fluorescence intensity of AGE stained cells were normalized to intensity of isotype stained cells.

3.2.8 Immunoblotting for RAGE and mDia1 Expression

After 24 hour culture, cells were cooled to 4°C and centrifuged at 400 x g for 7 minutes at 4°C. The cells were washed with cold PBS and centrifuged in a microcentrifuge for 10 minutes at 1500 rpm at 4°C. The pellets were resuspended in 100 µL of radio-immunoprecipitation (RIPA) buffer with 1:100 EDTA and 1:100 Halt protease inhibitor cocktail (all purchased from ThermoFisher Scientific). Tissue suspensions were rotated for 30 minutes at 4°C and then centrifuged for 20 minutes at 16,000 x g at 4°C. BCA was performed to determine total protein content (ThermoFisher Scientific). A western blot was performed to measure RAGE and mDia1 content using 10% SDS-PAGE gel electrophoresis (BIO-RAD). Equal amounts of protein were placed in each lane of the gel and subsequently transferred to nitrocellulose membranes. Non-specific binding was blocked by a 2-hour incubation at room temperature with 5% non-fat dry milk (BIO-RAD) in Tris-buffered saline containing 0.1% Tween-20 (TBST) (BIO-RAD). Primary rabbit polyclonal RAGE, mDia1 antibody, or GAPDH control (Millipore) was incubated with the membrane for 16 hours at 4°C in the blocking solution. After incubation, membranes were washed with TBST and then incubated for 1 hour with a secondary antibody goat anti-rabbit IgG HRP (Abcam) at room temperature. Membranes were washed in TBST and binding sites were identified by SuperSignal™ west picochemiluminescent assay (ThermoFisher Scientific) for 5 minutes. Bands were digitized with a scanner.

3.2.9 Baseline and SDF-1 Induced Superoxide Measurement

Twelve-well plates were coated with 125μL fibronectin solution (200μg/mL in PBS, Becton, Dickinson) per well for 1 hour at room temperature. HL-60 cells were washed in PBS and resuspended to $5x10^5$ cells/mL in PBS. Cells were then incubated with dihydroethidium (DHE) 1:1600 (Sigma-Aldrich) for 45 minutes at 37°C, washed in PBS, plated on the fibronectin-coated wells at a density of $5x10^5$ cells/well, incubated for 15 minutes at 37°C to allow for cell attachment, and washed in PBS. Each well was then visualized under an Olympus IX81® microscope to capture background images. The PBS was then removed and replaced with 250μL of PBS, after which images were taken every 30 seconds for 3.5 minutes. The wells were then replaced with 250μL of SDF-1 100 ng/mL after which images were taken every 30 seconds for 3.5 minutes. Images (five per replicate) were digitally captured and analyzed using ImageJ software (NIH) to determine mean fluorescence intensity after subtracting the background.

3.2.10 Statistics

All values are presented as means ± standard error of the mean (SEM). Multiple comparisons were carried out using one-way ANOVA followed by post-hoc analysis. Post-hoc tests are indicated in the figure legends.

3.3 RESULTS AND DISCUSSION

3.3.1 HL-60 Cell Migration to SDF-1 in D-glucose Culture with sRAGE Treatment

HL-60 cell migration was investigated in a cell culture system used to mimic the diabetic environment. Cells were cultured for 24 hours in IMDM media, IMDM with 25 mM added D-glucose or IMDM with 25 mM added L-glucose prior to migration testing (figure 3.1). In the absence of SDF-1, approximately 5% of cells migrate to the bottom of the transwell chamber, regardless of culture condition. When 100ng/mL SDF-1 was added to the transwell, the fraction of cells that migrated increased 3-fold compared to

regular media. This increase was suppressed in hyperglycemic medium, but unaffected in the L-glucose “decoy” medium, consistent with the hypothesis that D-glucose mediated inhibition requires metabolic processing of the glucose. When sRAGE was added to the migration assay, the migratory response was no longer suppressed in hyperglycemic medium. sRAGE did not affect SDF-1 directed migration in cells cultured with media only or media with L-glucose. sRAGE alone did not induce significant cell

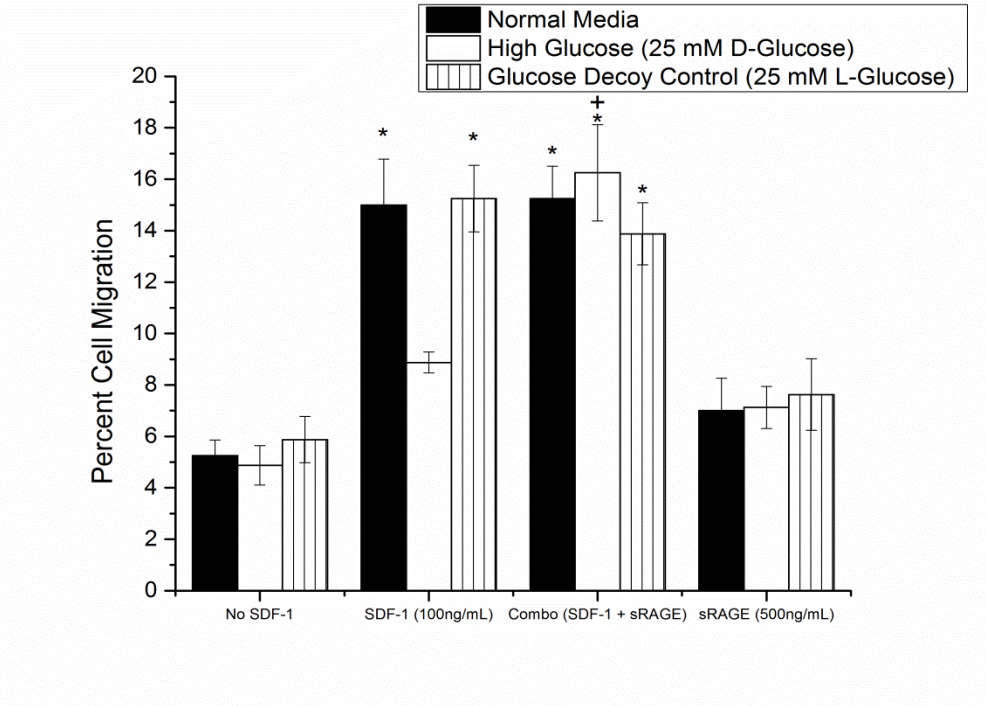

Figure 3.1 HL-60 Migration in the Presence of High Glucose. HL-60 cells (10^5 in 100µL) were placed on top of a transwell in a 24-well plate after 24 hours of plain IMDM media, high glucose (media + 25 mM D-glucose), or glucose decoy (media + 25 mM L-glucose) culture. The bottom of the well was filled with 600µL of basal IMDM media or media containing 100 ng/mL SDF-1, 100 ng/mL SDF-1 + 500 ng/mL sRAGE, or 500 ng/mL sRAGE. Data shown are the number of cells that migrated across the membrane normalized to the number of cells added to the well. N=6. (*: $p < 0.01$ compared to No SDF-1 control, +: $p < 0.05$ compared to SDF-1, one way ANOVA, Fisher’s LSD post-test).

migration. While the culture conditions attribute to the difference in migration, viability of cells, which was 93.4 ± 1.5% in plain cell media, was not affected by added L- or D-glucose, which had viabilities of 94.0 ± 3.0% and 94.1 ± 1.0%, respectively (N=6). Furthermore, expression of SDF-1 receptor CXCR4 was unchanged in media supplemented with D-glucose (figure 3.2), indicating that change in migratory function did not correlate with a change in the amount of CXCR4 receptor.

3.3.2 Primary Mononuclear Cell Migration

Comparable trends were observed using mouse peripheral mononuclear white blood cells in the transwell assay (figure 3.3). Baseline migration, in the absence of SDF-1, was around 35% with the primary cells; this increased to 75% in the presence of SDF-1. Media supplemented with D-glucose again suppressed migration compared to

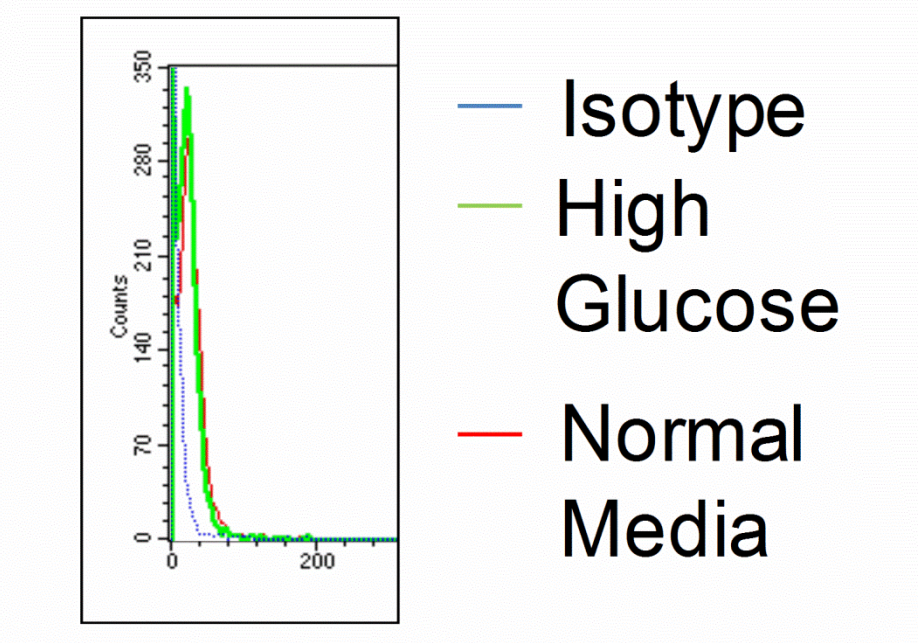

Figure 3.2 HL-60 CXCR4 Expression. After 24 hours of plain IMDM media or high glucose (media + 25 mM D-glucose) culture, 100,000 cells per condition were incubated with anti-cxcr4 antibody or isotype control and run through FACSCalibur flow cytometer. Data shown are counts vs. FL-4 fluorescence. Fluorescence gated at 5%. N=6.

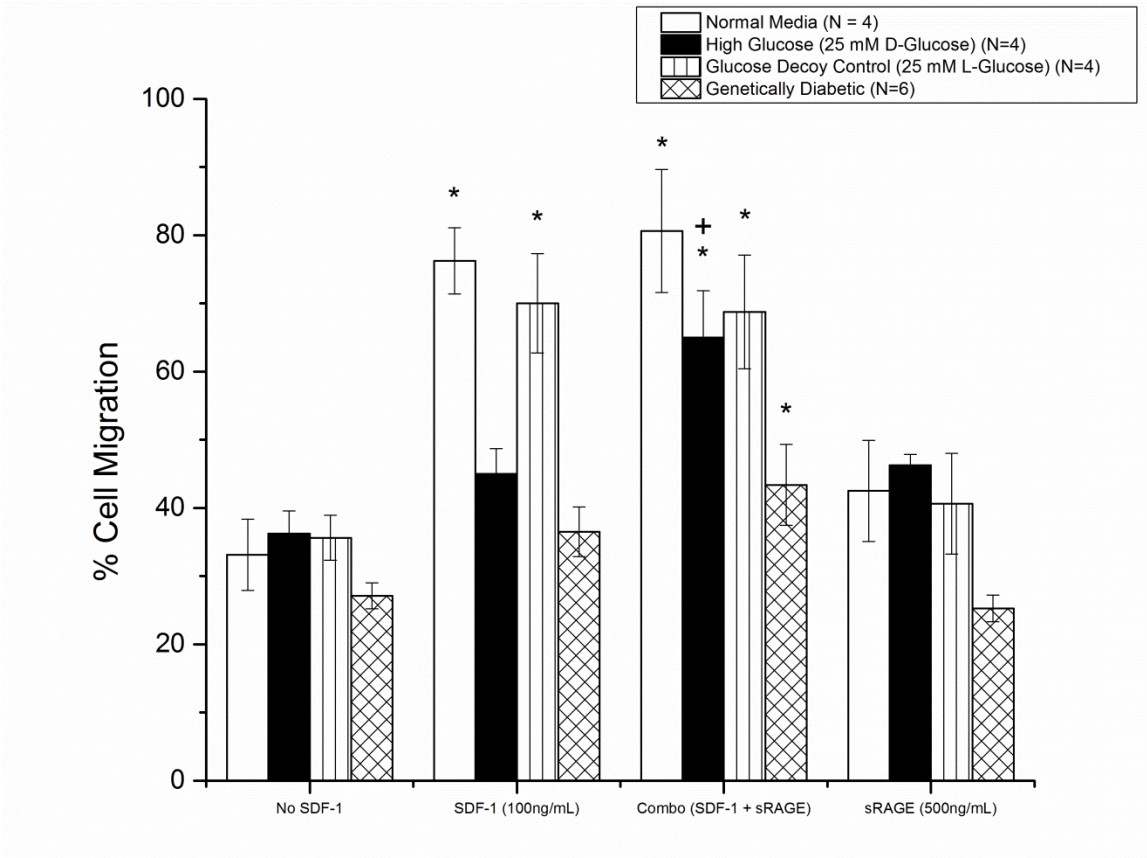

Figure 3.3 Primary Cell SDF-1 Directed Migration in High Glucose. Mouse mononuclear white blood cells from wild type or Lepr^{db} genetically diabetic mice (10^5 in 100µL) were placed on top of a transwell in a 24-well plate after 24 hours of plain IMDM media, high glucose (media + 25 mM D-glucose), or glucose decoy (media + 25 mM L-glucose) culture. The bottom of the well was filled with 600µL of basal IMDM media or media containing 100 ng/mL SDF-1, 100 ng/mL SDF-1 + 500 ng/mL sRAGE, or 500 ng/mL sRAGE. Data shown are the number of cells that migrated across the membrane normalized to the number of cells added to the well. (*: $p < 0.01$ compared to No SDF-1 control, +: $p < 0.05$ compared to SDF-1, one way ANOVA, Fisher's LSD post-test).

controls, which was reversed by the addition of sRAGE. These data were obtained from *in vitro* induced conditions over a short timescale; we also investigated the response of cells from 10-week old $Lepr^{db}$ diabetic mice, which better approximate diabetes. Mononuclear cells exhibited lower baseline migration (27%) than cells from normal mice, and the response to SDF-1 was marginal. sRAGE increased the migration to ~45% ($p < 0.05$ vs. baseline). The primary cell model was consistent with that of the diabetic culture model, which we used thereafter.

3.3.3 AGE, mDia1, and RAGE Expression

Since the effects of increased glucose were reversed by sRAGE, we hypothesize that the impaired SDF-1 directed migration was due to AGE-mediated signaling. Therefore, the accumulation of AGEs was measured in HL-60s using immunohistochemistry after 24 hour cultures (figure 3.4). Cells cultured in plain media had virtually no detectible amount of AGEs, while cells cultured in media with D-glucose had a two-fold increase in the amount of AGEs. Cells cultured in media with L-glucose slightly increased the amount of AGEs, though it was not significant. The expression of RAGE and its intracellular signaling partner mDia1 were measured by western blot, with no differences seen among groups (figure 3.5). This observation suggests that, though AGE levels were strongly influenced by the environment, there was no such change on the receptor apparatus. Additionally, sRAGE did not affect the receptor expression.

3.3.4 SDF-1 and sRAGE effect on ROS

AGE binding to RAGE is known to lead to the generation of ROS, and, chemokine signals, such as SDF-1, produce and utilize ROS in their migration pathway. Traditionally, manipulation of ROS production has led to changes in cellular migration. We hypothesize that, in the presence of AGEs, a higher baseline of ROS levels in the cells may prevent the generation of an SDF-1-mediated burst of ROS. Using

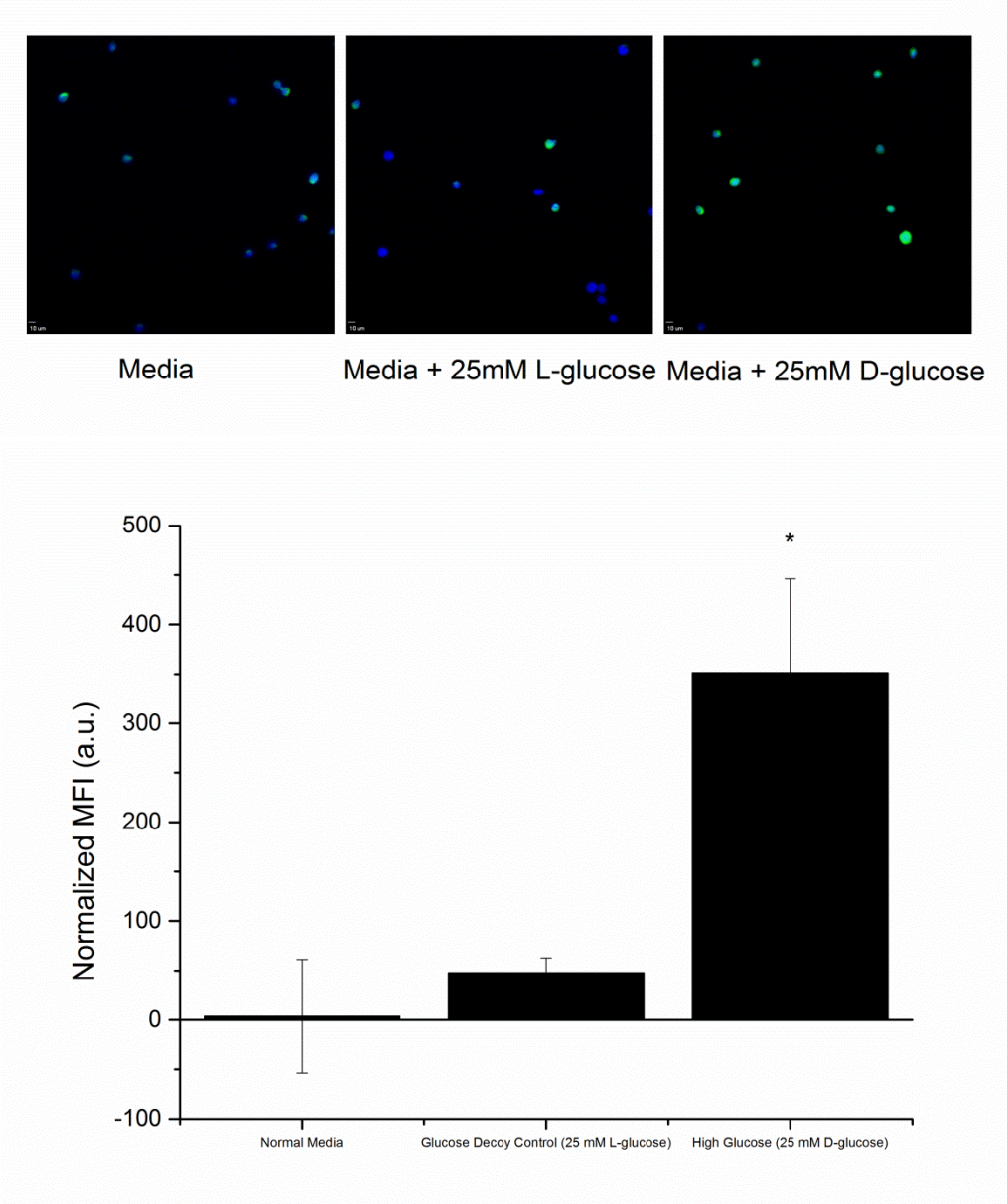

Figure 3.4 AGE Content in High Glucose Culture. HL-60 cells were fixed with 4% paraformaldehyde and stained with AGE primary antibody and fluorescein conjugated secondary antibody. (TOP) Representative images of HL-60 cells stained with AGE antibody (Green) and DAPI (blue). (BOTTOM) Data shown is the mean fluorescence intensity of each group normalized to the isotype control. N =4. (*: $p < 0.01$, one way ANOVA, Fisher's LSD post-test).

dihydroethidium as a superoxide reporter, we observed that HL-60 cells cultured in media with D-glucose had significantly higher levels of baseline ROS than cells cultured in plain media (figure 3.6). Furthermore, sRAGE decreased baseline ROS levels in the D-glucose media cultured cells similar to levels of the plain media cultured cells. Cells cultured with L-glucose had a higher baseline ROS level than plain media cultured cells, though both were much lower than the D-glucose cultured cells, and the difference was not significant. When SDF-1 was added, a spike in ROS was seen in media and media supplemented with L-glucose cultured cells. In contrast, cells cultured with D-glucose media did not induce a spike in ROS when SDF-1 was added. Addition of sRAGE to the D-glucose cultured cells restored the SDF-1 spike and led to a bigger change than the

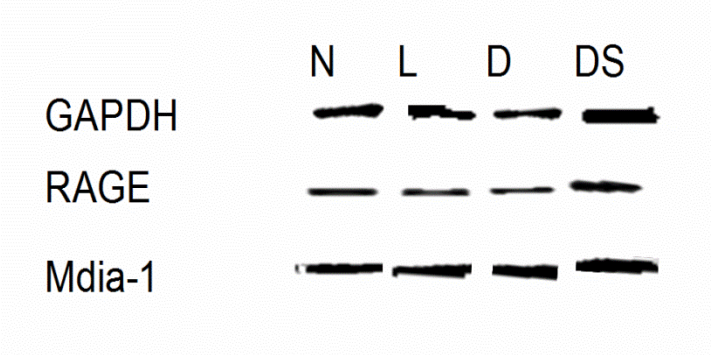

Figure 3.5 RAGE and MDia1 Expression in High Glucose Culture. Protein from 24 hour HL-60 cell culture was isolated and aliquots of protein were normalized to total protein via BCA assay and run through gel electrophoresis. Gels were transferred to nitrocellulose, were they were incubated with GAPDH antibody control, polyclonal RAGE antibody, or polyclonal mDIA1 antibody. Bands were obtained and digitized for cells cultured in plain IMDM media (N), media + 25 mM L-glucose (L), media + 25 mM D-glucose (D), and media + 25 mM D-glucose + 500 ng/mL sRAGE (DS). Data shown are representative blots for each condition.

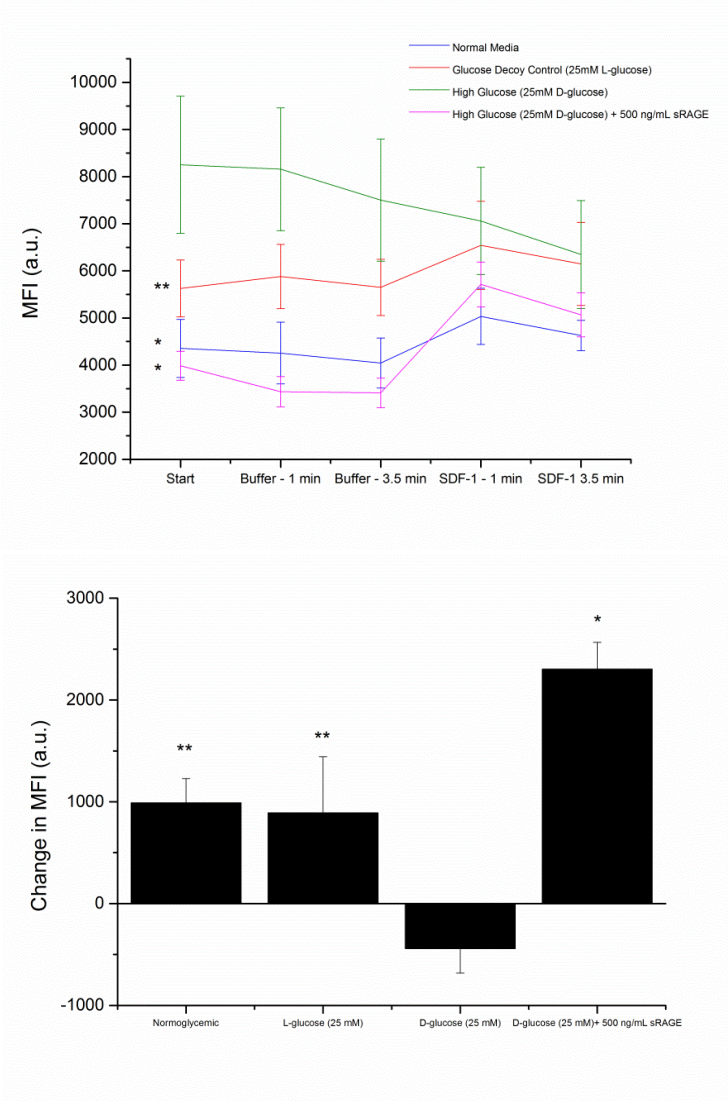

Figure 3.6 Superoxide Content in High Glucose Culture. HL-60 cells were stained with dihydroethidium (DHE) and plated in 12-well fibronectin-coated plates at $5x10^5$ cells/well. Baseline fluorescent images were taken and cells were then PBS buffer was added. Images were taken 1 min and 3.5 min post-treatment. The cells were then switched to treatment consisting of 250 µL 100ng/mL SDF-1. Images were taken 1 min and 3.5 min post-treatment. (TOP) Mean fluorescence intensity (MFI) per well as a function of time as quantified by digital image analysis. (B) Change in MFI at 3.5 min post treatment after addition of SDF-1. N=5. (*: $p < 0.01$, **: $p < 0.05$, one way ANOVA, Fisher's LSD post-test).

plain media control. The SDF-1-mediated intracellular signaling cascade, which normally results in a ROS burst, is inhibited by media supplemented with D-glucose, and that response is restored by sRAGE.

3.4 CONCLUSION

This chapter investigates the mechanism responsible for the decreased SDF-1 directed migration in the presence of a simulated diabetic environment (high glucose) and the reversal of the impaired migration with sRAGE. In both primary mouse cells and our model HL-60 cell line system, impaired SDF-1 directed transwell migration due to high glucose was restored when sRAGE was added. Even in cells from genetically diabetic mice, which see a prolonged diabetic environment (versus just 24 hours in culture), had a significant increase in migration when treated with sRAGE. Within the 24 hour culture, HL-60 cells remained >90% viable. While the addition of glucose increased the AGEs in the environment significantly, both SDF-1 and AGE receptor expression (CXCR4 and RAGE, respectively) were unchanged through the 24 hour culture period.

However, there was an interesting intersection in signaling between the production of ROS and cell migration, where an increase in ROS has traditionally had a negative impact on migration. This was confirmed in our studies, where media with added D-glucose culture condition increase ROS compared to the media and media with L-glucose added cells.There was also no spike in ROS when SDF-1 is added to the D-glucose media cultured cells, which was seen in the control conditions. In the condition where sRAGE was added along with D-glucose for the 24 hour culture, the baseline ROS level decreased back to the levels of the control. When SDF-1 was then added, the ROS spike was restored and, in fact, even larger than the controls. Therefore, the simulated diabetic environment may desensitize the cell to ROS-inducing chemokines, such as SDF-1.

3.5 REFERENCES

1 H. Li, X. Zhang, X. Guan, X. Cui, Y. Wang, H. Chu, and M. Cheng, Advanced Glycation End Products Impair the Migration, Adhesion and Secretion Potentials of Late Endothelial Progenitor Cells, *Cardiovasc Diabetol,* 11 (2012), 46.

2 M. T. Goova, J. Li, T. Kislinger, W. Qu, Y. Lu, L. G. Bucciarelli, S. Nowygrod, B. M. Wolf, X. Caliste, S. F. Yan, D. M. Stern, and A. M. Schmidt, Blockade of Receptor for Advanced Glycation End-Products Restores Effective Wound Healing in Diabetic Mice, *Am J Pathol,* 159 (2001), 513-25.

3 T. E. Restivo, K. A. Mace, A. H. Harken, and D. M. Young, Application of the Chemokine Cxcl12 Expression Plasmid Restores Wound Healing to near Normal in a Diabetic Mouse Model, *J Trauma,* 69 (2010), 392-8.

4 K. A. Gallagher, Z. J. Liu, M. Xiao, H. Chen, L. J. Goldstein, D. G. Buerk, A. Nedeau, S. R. Thom, and O. C. Velazquez, Diabetic Impairments in No-Mediated Endothelial Progenitor Cell Mobilization and Homing Are Reversed by Hyperoxia and Sdf-1 Alpha, *J Clin Invest,* 117 (2007), 1249-59.

5 M. Morcos, A. A. Sayed, A. Bierhaus, B. Yard, R. Waldherr, W. Merz, I. Kloeting, E. Schleicher, S. Mentz, R. F. Abd el Baki, H. Tritschler, M. Kasper, V. Schwenger, A. Hamann, K. A. Dugi, A. M. Schmidt, D. Stern, R. Ziegler, H. U. Haering, M. Andrassy, F. van der Woude, and P. P. Nawroth, Activation of Tubular Epithelial Cells in Diabetic Nephropathy, *Diabetes,* 51 (2002), 3532-44.

6 F. Barbieri, A. Bajetto, and T. Florio, Role of Chemokine Network in the Development and Progression of Ovarian Cancer: A Potential Novel Pharmacological Target, *J Oncol,* 2010 (2010), 426956.

7 R. L. Lee, J. Westendorf, and M. R. Gold, Differential Role of Reactive Oxygen Species in the Activation of Mitogen-Activated Protein Kinases and Akt by Key Receptors on B-Lymphocytes: Cd40, the B Cell Antigen Receptor, and Cxcr4, *J Cell Commun Signal,* 1 (2007), 33-43.

8 A. Sutton, V. Friand, S. Brule-Donneger, T. Chaigneau, M. Ziol, O. Sainte-Catherine, A. Poire, L. Saffar, M. Kraemer, J. Vassy, P. Nahon, J. L. Salzmann, L. Gattegno, and N. Charnaux, Stromal Cell-Derived Factor-1/Chemokine (C-X-C Motif) Ligand 12 Stimulates Human Hepatoma Cell Growth, Migration, and Invasion, *Mol Cancer Res,* 5 (2007), 21-33.

9 V. P. Singh, A. Bali, N. Singh, and A. S. Jaggi, Advanced Glycation End Products and Diabetic Complications, *Korean J Physiol Pharmacol,* 18 (2014), 1-14.

10 A. M. Vincent, J. W. Russell, P. Low, and E. L. Feldman, Oxidative Stress in the Pathogenesis of Diabetic Neuropathy, *Endocr Rev,* 25 (2004), 612-28.

11 F. Toure, G. Fritz, Q. Li, V. Rai, G. Daffu, Y. S. Zou, R. Rosario, R. Ramasamy, A. S. Alberts, S. F. Yan, and A. M. Schmidt, Formin Mdia1 Mediates Vascular Remodeling Via Integration of Oxidative and Signal Transduction Pathways, *Circ Res,* 110 (2012), 1279-93.

12 H. Hattori, K. K. Subramanian, J. Sakai, Y. Jia, Y. Li, T. F. Porter, F. Loison, B. Sarraj, A. Kasorn, H. Jo, C. Blanchard, D. Zirkle, D. McDonald, S. Y. Pai, C. N. Serhan, and H. R. Luo, Small-Molecule Screen Identifies Reactive Oxygen Species as Key Regulators of Neutrophil Chemotaxis, *Proc Natl Acad Sci U S A,* 107 (2010), 3546-51.

13 J. A. van Aalst, D. M. Zhang, K. Miyazaki, S. M. Colles, P. L. Fox, and L. M. Graham, Role of Reactive Oxygen Species in Inhibition of Endothelial Cell Migration by Oxidized Low-Density Lipoprotein, *Journal of Vascular Surgery,* 40 (2004), 1208-15.

14 C. C. Lan, I. H. Liu, A. H. Fang, C. H. Wen, and C. S. Wu, Hyperglycaemic Conditions Decrease Cultured Keratinocyte Mobility: Implications for Impaired Wound Healing in Patients with Diabetes, *Br J Dermatol,* 159 (2008), 1103-15.

4. CHAPTER 4: DEVELOPMENT OF SDF-1 LIPOSOMES FOR IN VIVO DELIVERY USING ACELLULARIZED DERMIS

Note: This chapter is reproduced from the following publication:

Przyborowski Olekson M, Faulknor R, Bandekar A, Sempkowski M, Hsia HC, Berthiaume F. Liposomally Enhanced Acellular Dermis for Diabetic Wound Healing. *Wound Repair and Regeneration (Submitted 05/2014).*

A. Bandekar and M. Sempkowski prepared liposomes and directly produced data for encapsulation efficiency (in text) and liposome charge and size (table 4.1).

4.1 INTRODUCTION

In addition to improving growth factor action, the goal of this project is to improve growth factor persistence at the wound site. In wound treatment development, growth factors have been successful in pre-clinical animal studies while having mixed results in the clinic. The lone FDA-approved growth factor treatment is Regranex®, a platelet-derived growth factor (PDGF) topical gel, which has shown to be effective in treating diabetic ulcers[1]. Multiple applications of Regranex® are often necessary due to the high levels of proteinases degrading the exogenous growth factor away[2]. However, it has been tagged with an FDA black box warning for increased malignancy after multiple applications. Therefore, there exists a need to develop drug delivery systems (DDS) to deliver growth factors topically to chronic wounds. The goal of this chapter is to create an SDF-1 liposome drug delivery system to be delivered to the wound in already FDA-approved decellularized matrices.

The SDF-1 liposomes are delivered to the wound site using decellularized matrices, which, in general, are manufactured by processing explanted whole tissues to remove all cells while keeping the extracellular matrix more or less intact, and are currently being used in the clinic to help regenerate skin, pulmonary valves, and bone[3]. A few recent studies have suggested that supplementing such materials with exogenous

growth factors may be beneficial[4]. For example, previous studies have shown that exogenous free stromal-derived factor-1 (SDF-1) enhances the rate of healing of excisional skin wounds in mice[5]. Another report showed that sustained local release of VEGF by nanoparticles enhanced tissue in-growth in implanted decellularized blood vessels[6]. Because impaired blood flow is common in diabetic wounds, vascularization of the matrices can be slow; therefore, the use of SDF-1 liposomes can also help with matrix engraftment[7].

While there are many drug delivery system materials available, liposomes (lipid vesicles self-assembled in a water phase), have many attributes that make them an optimal choice for delivering growth factors. Like many other DDS materials, the main function of the liposome is to extend the half-life of the drug at the delivery site, serving as a local reserve of the factor[8]. Liposomes have particular advantages such as the ability to entrap materials, nanoscale assembly, and the ability to be modified to enhance certain attributes, like charge[9]. They have been used in acute and diabetic skin wounds in prior literature, in general showing the liposome plus drug combinations improve drug delivery and wound closure compared to treatment with the free drug. These studies have typically aimed to improve the half-lives of molecules which are rapidly used or degraded in the body. In Roesken, et al., buflomedil, a vasodilator, was successfully encapsulated in liposomes to extend the half-life of the drug. The buflomedil liposomes successfully improved wound closure in 2.5 mm diameter wounds and increased vascularization in mice[10]. In Wang et al., liposome encapsulated ATP, which in free form also has a short half-life, was successful in improving 6.0 mm diameter ear wound closure in diabetic rabbits[11].

In this study, we developed nanosized liposome-bound SDF-1 (SDF-1 liposomes) by associating negatively charged liposomes with the positively charged SDF-1. The majority of the positive charges on SDF-1 are located in the central β-sheet

region of the peptide, while the N-terminal region contains the binding sequence for its cognate receptor CXCR4[12, 13]. Therefore, the liposomes have the potential to bind SDF-1 while keeping the N-terminal sequence available for signaling. The resulting particles had a small size distribution and a high (>80%) SDF-1 encapsulation efficiency. To ensure success *in vivo*, the function of the SDF-1 liposomes were first tested *in vitro* for the ability to induce cell migration and SDF-1 signaling. The particles were also loaded into decelluarized matrices for delivery to the wound.

4.2 METHODS

4.2.1 Preparation and Characterization of SDF-1 Liposomes

Liposomes were formed using previously published methods[14]. Briefly, 10μmol total lipid was combined in chloroform in a 25 mL round bottom flask at a mole ratio of 7:2:1 of DSPC:cholesterol:DSPA. For tracking, 1 mole % DPPE-rhodamine was added. All lipids were purchased from Avanti Polar Lipids. Chloroform was evaporated in a rotovapor for 10 minutes at 55°C followed by exposure to nitrogen for 5 minutes. The lipid film was hydrated in 1 mL of HEPES-sucrose buffer (pH = 7.4, Sigma-Aldrich) for 2 hours with final lipid concentration of 10 mM. The lipid suspension was extruded 21 times through two sizes of polycarbonate membranes, first with two stacked 200 nm pore size, and then with two stacked 100 nm pore size in an 80°C water bath. Liposomes were diluted to 100μM lipid and SDF-1 (R&D Systems) in HEPES-sucrose buffer was then added to the liposomes under vortexing at a molar ratio of 1:9 with respect to DSPA. Transmission electron microscopy (TEM) images were obtained at the Electron Imaging Facility of the Department of Life Sciences at Rutgers University. Samples were prepared with uranyl acetate for negative staining.

Liposome size was determined by dynamic light scattering and zeta potential determined based on electrophoretic mobility and Smoluchowski model using a

Zetasizer NanoSeries (Malvern, Instruments, Ltd, Worcestershire, UK) based on prior studies[15].

To measure the efficiency of incorporation of the SDF-1 into liposomes, the SDF-1 liposomes were eluted on a 10 mL Sepharose 4B size exclusion chromatography (SEC) column (Sigma-Aldrich) eluted with HEPES-sucrose buffer. Total protein content eluted with liposomes was determined using a micro-BCA (ThermoFisher Scientific) and was quantitated using a standard curve of SDF-1. Incorporation efficiency was calculated as the ratio of SDF-1 associated within liposomes over the initial amount of SDF-1 used in the preparation of the liposomes.

4.2.2 Cell Culture

HL-60 cells were purchased from American Type Culture Collection (ATCC). Cultures were maintained in T-75 flasks (Becton, Dickinson) at 10^5 - 10^6 cells/mL in Iscove's Modified Dulbecco's Medium (IMDM) supplemented with 20% Fetal Bovine Serum (FBS) and penicillin-streptomycin (Life Technologies).

4.2.3 Transwell Migration Assay

HL-60 cells were suspended at 10^6 cells/mL in IMDM supplemented with 20% FBS. A total of 10^5 cells in 100μL medium were placed on top of a 24-well plate transwell porous insert (transparent polyethylene terephthalate (PET) membrane, 8μm pores, Corning). The bottom of the well was preloaded with 600μL of IMDM or IMDM supplemented with 100 ng/mL SDF-1, 100 ng/mL SDF-1 in liposomes, or the same amount of empty liposomes (1.13μM lipids). Plates were incubated at 37°C and harvested after 1, 2, and 4 hours. The number of cells that passed through to the bottom well were counted using a hemacytometer (Hausser) and normalized to the initial number of added cells (10^5 cells).

4.2.4 Intracellular Calcium Ion Release Assay

Twelve-well plates were coated with 125μL fibronectin solution (200μg/mL in PBS, Becton-Dickinson) per well for 1 hour at room temperature. HL-60 cells were washed in PBS and resuspended to 10^6 cells/mL in PBS. Cells were then incubated with 4μM fluo-4 AM (LifeTechnologies) for 45 minutes at 37°C, washed in PBS, plated on the fibronectin-coated wells at a density of $5x10^5$ cells/well, incubated for 15 minutes at 37°C to allow for cell attachment, and washed in PBS. Each well was then visualized under an Olympus IX81® microscope to capture background images. The PBS was then removed and replaced with 250μL of test solution (plain PBS, 100 ng/mL SDF-1, 100ng/mL SDF-1 liposomes, or empty liposomes in PBS), after which images were taken every 30 seconds for 3.5 minutes. Then, the test solution was removed and the cells were incubated with 250μL ionomycin (1μg/mL in PBS) and imaged again every 30 seconds for 3.5 minutes. Images were digitally captured and analyzed using ImageJ software (NIH) to determine mean fluorescence intensity after subtracting the background.

4.2.5 Distribution of SDF-1 Liposomes in Acellular Dermis

Acellular dermis (Alloderm®, LifeCell) was hydrated in PBS, cut into 5mm diameter punches, and each punch was pushed to the bottom of a well in a 96-well plate. Baseline confocal images were taken (5 images per well, 20μm apart) throughout the entire thickness (approximately 200μm) of the dermis using an Olympus IX81® confocal microscope. Then, 100μL of SDF-1 liposomes, empty liposomes, or plain PBS were added on top of each punch. These liposomes were labeled with 1% DPPE-rhodamine for fluorescence detection. The well plate was placed on a plate shaker (500 rpm, ThermoFisher Scientific) for 1 hour at room temperature. Confocal images of each well were taken using the same coordinates as that taken before SDF-1 loading. Mean fluorescence intensity was quantified using ImageJ (NIH) software and normalized to the intensity of the initial baseline images.

4.2.6 Statistics

All values are presented as means ± standard error of the mean (SEM). Multiple comparisons were carried out using one-way ANOVA followed by post-hoc analysis. Post-hoc tests are indicated in the figure legends.

4.3 RESULTS AND DISCUSSION

4.3.1 Characterization of SDF-1 Liposomes

Freshly made SDF-1 liposomes measured ~150 nm in diameter, compared to ~100 nm for empty liposomes (table 4.1). The polydispersity index was low (less than 0.1), indicating a narrow size distribution. The net charge of the SDF-1 liposomes was nearly equal to zero, indicating a close to one-to-one match in the number of charges from the DSPA (one negative charge per molecule) and the number of charges on the SDF-1 (9 exposed positive charges per molecule). In contrast, the empty liposomes recorded a net charge of -10mV. Encapsulation efficiency was determined to be 80.2 ± 3.4% (n=4), thus indicating a high yield of SDF-1 incorporation into the nanoparticles. SDF-1 liposomes imaged by transmission electron microscopy (TEM) revealed spherical particles of about 100nm in size (figure 4.1).

Empty Liposomes (Before Adding SDF-1)		
Size (nm)	**Polydispersity Index**	**Zeta Potential (mV)**
109 ± 2	0.06 ± 0.02	-10.10 ± 1.10
SDF-1 Liposomes (After Adding SDF-1)		
Size (nm)	**Polydispersity Index**	**Zeta Potential (mV)**
153 ± 8	0.07 ± 0.03	-0.60 ± 0.98

Table 4.1 SDF-1 Liposome Characterization. Liposomes were sized using dynamic light scattering before and after SDF-1 was added. Zeta potential was also determined. N=4.

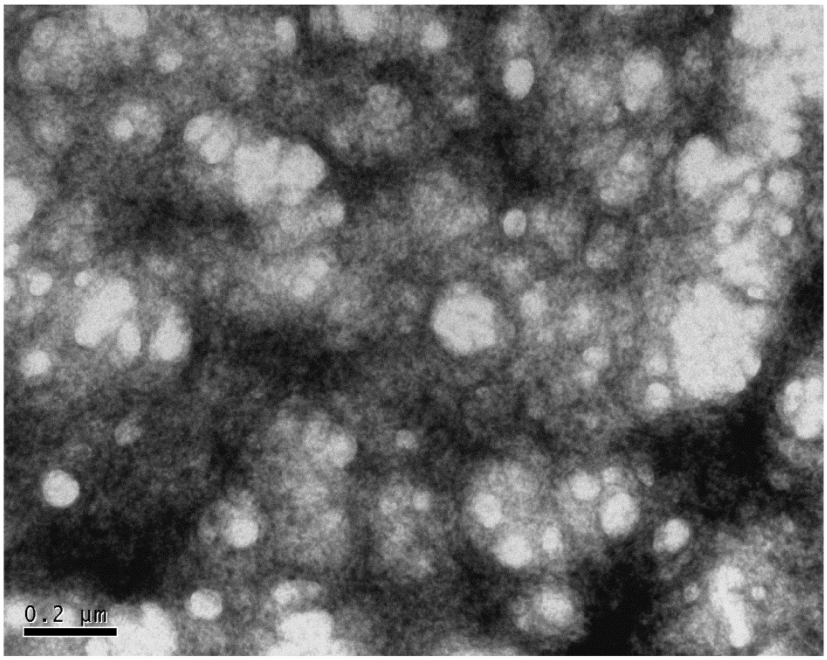

Figure 4.1. TEM of SDF-1 Liposomes. SDF-1 Liposome Morphology was viewed by TEM with negative stain uranyl acetate. Bar size = 200 nm.

SDF-1 liposomes were compared with free SDF-1 for their ability to induce physiological responses. First, SDF-1 liposomes were tested for chemotactic activity towards HL-60 cells. As expected, free SDF-1 triggered a time- and dose-dependent migration response in the HL-60 cells in a transwell assay (Figure 4.2). In comparison, SDF-1 liposomes induced 30% lower migration after 1 hour incubation, but migration measured at 2 and 4 hours was indistinguishable from that induced by free SDF-1. Empty liposomes did not enhance migration above baseline observed in controls maintained in basal medium. To probe whether the delay in migration when using the SDF-1 liposomes could be due to a lower effective dose of the SDF-1 and/or a functional delay in SDF-1-mediated signaling, we investigated the ability of SDF-1 liposomes to induce a burst in intracellular calcium ion. Calcium transients were monitored using fluo4 fluorescence (Figure 4.3). Addition of free SDF-1 induced a sudden burst in fluo4

fluorescence signal, after which the level decreased slightly although it remained above baseline for the next 3.5 minutes of observation, at which point calcium ionophore was added as positive control, causing a huge burst in fluorescence. SDF-1 liposomes also induced a rapid increase in fluo4 signal, with no significant differences in

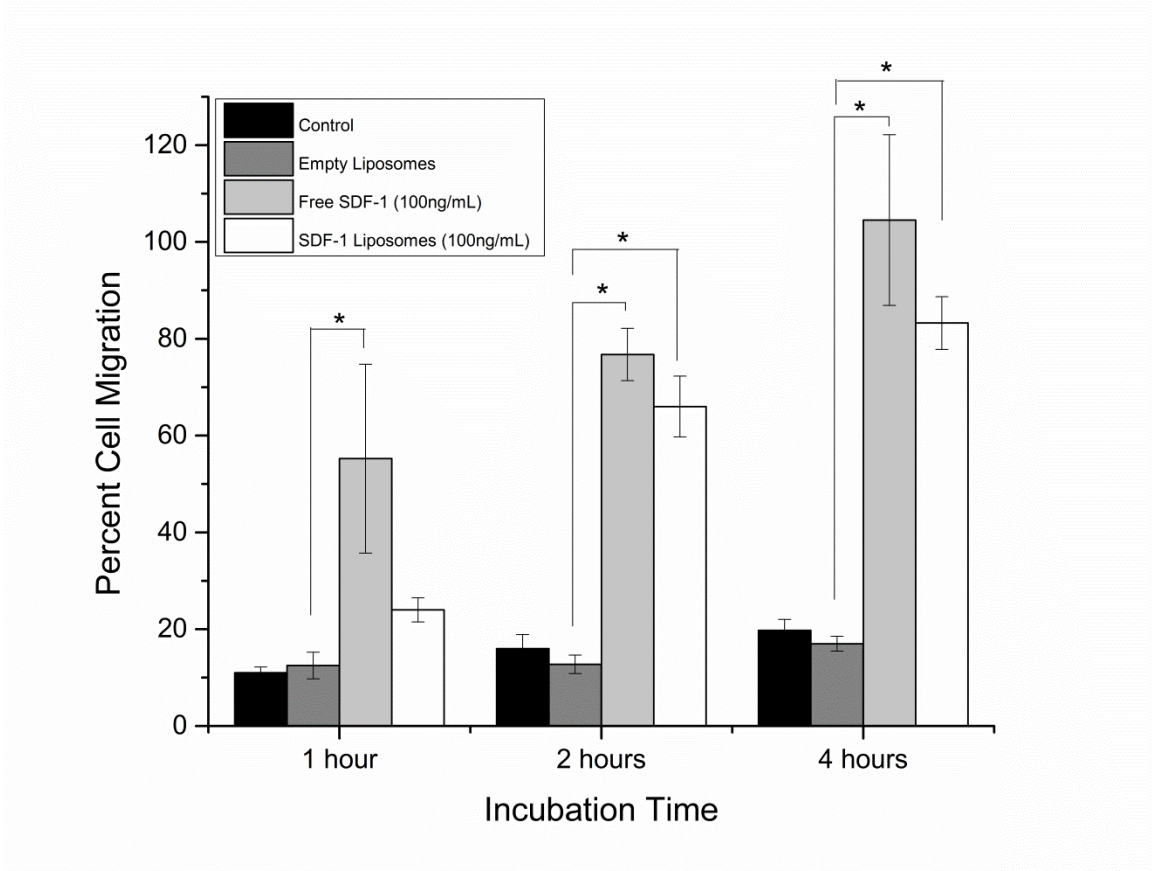

Figure 4.2. HL-60 Migration to SDF-1 Liposomes. HL-60 cells (10^5 in 100µL) were placed on top of a Transwell in a 24-well plate to measure chemotactic response to SDF-1 liposomes. The bottom of the well was filled with 600µL of basal medium (control), medium with 1.13µM empty liposomes, medium with 100 ng/mL SDF-1, or medium with 100 ng/mL SDF-1 bound to 1.13µM liposomes. Data shown are the number of cells that migrated across the membrane normalized to the number of cells added to the well. N=5. (*: $p < 0.01$, one way ANOVA, Fisher's LSD post-test).

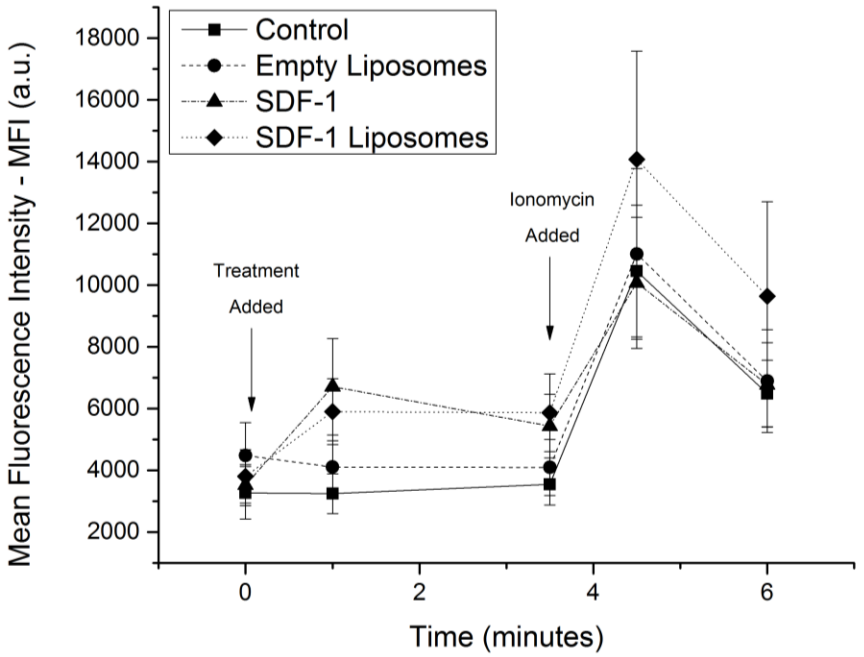
Control
Empty Liposomes
SDF-1
SDF-1 Liposomes
Mean Fluorescence Intensity - MFI (a.u.)
Time (minutes)
Treatment Added
Ionomycin Added
18000
16000
14000
12000
10000
8000
6000
4000
2000
0
2
4
6

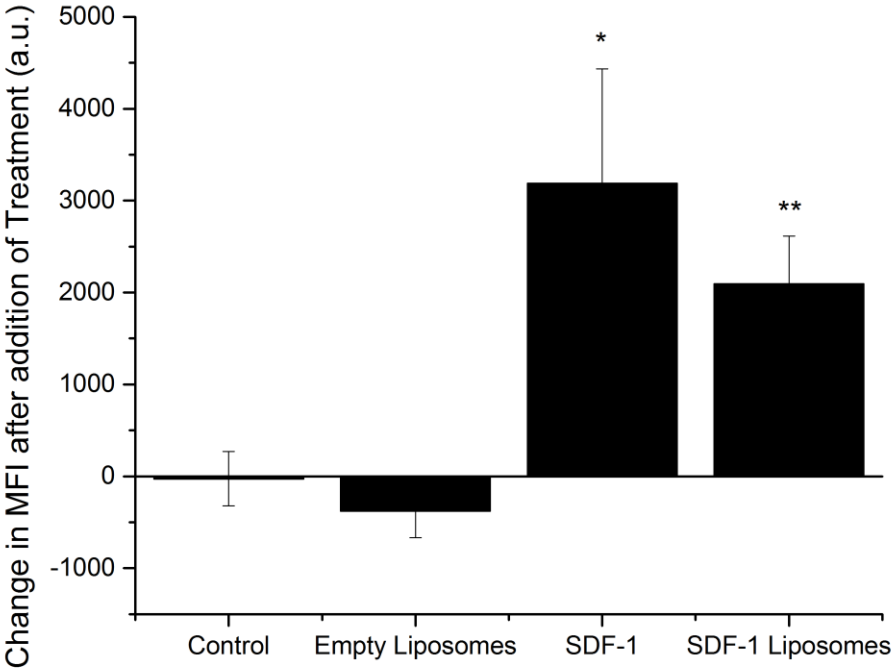
Change in MFI after addition of Treatment (a.u.)
5000
4000
3000
2000
1000
0
-1000
*
**
Control
Empty Liposomes
SDF-1
SDF-1 Liposomes

Figure 4.3. Calcium Ion Response Induced from Free SDF-1 and SDF-1 Liposomes. HL-60 cells were stained with calcium indicator and plated in 12-well fibronectin-coated plates at $5x10^5$ cells/well. Baseline fluorescent images were taken and cells were then switched to treatment consisting of 250μL PBS (control), PBS with 1.13μM empty liposomes, PBS with 100ng/mL SDF-1, or PBS with 100ng/mL SDF-1 bound to 1.13 μM liposomes. Images were taken 1 min and 3.5 min post-treatment. Ionomycin (1μg/mL) was then added to cause maximal intracellular calcium release. (TOP) Mean Fluo-4 fluorescence intensity (MFI) per well as a function of time as quantified by digital image analysis. (BOTTOM) Change in MFI at 1 min post treatment vs. initial value. N=5. (*: $p < 0.01$, **: $p < 0.05$, one way ANOVA, Fisher's LSD post-test).

behavior compared to free SDF-1. Addition of PBS or empty liposomes did not cause any fluorescence change, indicating that the calcium responses reflected SDF-1 mediated effects.

One attractive feature of the SDF-1 bound liposome system is the mechanism of association between liposomes and SDF-1 is based on electrostatic attraction between exposed positive charges on the SDF-1 molecule and the negative charges of the phospholipid head groups. Thus, the protocol for generating SDF-1 bound liposomes was extremely simple and led to a high incorporation efficiency of SDF-1 (>80%). The neutralization of liposome charge after incubation with SDF-1 (Table 4.1) suggests that this binding did occur. Also, because the positive SDF-1 charges are positioned away from the CXCR4 binding site, the SDF-1 liposomes still have the potential to bind CXCR4, which is consistent with our observation that the SDF-1 bound to liposomes was nearly equally effective in triggering chemotactic and intracellular calcium signaling responses in vitro compared to free SDF-1. The only difference observed in this respect was the delayed HL-60 chemotaxis in response to SDF-1 bound liposomes compared to that induced by a similar amount of free SDF-1. It is possible that this delay is due to the comparatively large size of the liposomes, which may exhibit slower diffusivity and take longer to form a proper chemotactic gradient of SDF-1 available for binding across the Transwell membrane. The delay was only on the order of a few hours, which is likely of no significance in vivo where the tissue repair process takes days to weeks.

4.3.2 Incorporation of SDF-1 Liposomes into Acellular Dermis

To use the SDF-1 liposomes for wound healing applications, they were incorporated into commercially available microporous acellular dermis (Alloderm®). To assess SDF-1 liposome distribution within the acellular dermis, empty liposomes as well as SDF-1 containing liposomes were made using rhodamine tagged phospholipids. Fluorescence intensity observed at each optical section was uniformly flat, and did not

change as a function of depth into the skin substitute, indicating complete penetration of the liposomes into the material. Furthermore, fluorescence intensity was directly proportional to the dose of liposomes (Figure 4.4). The size of the SDF-1 bound liposomes, which was around 150 nm, was uniform and well below the typical pore size of decellularized matrices, which is of the order of 10μm or more. Because of the small size, it was therefore easy to fully and uniformly percolate the acellular dermis with the SDF-1 liposomes. This in turn, ensured that the SDF-1 liposomes were delivered uniformly to the wound surface.

4.4 CONCLUSION

This study contains the creation and *in vitro* testing of SDF-1 bound liposomes. The lipid composition of the liposome contained DSPA lipids, DSPC lipids, and cholesterol. The determination of using 10% DSPA was because the negative charges of the DSPA at this molar ratio balance the positive charges on the amount of SDF-1 used (0.88 μg). The remaining materials (neutrally charged DSPC and cholesterol) were used to stabilize the liposomes. Nanosized liposomes were created, and they retained high levels of the starting amount of SDF-1. In addition, they exhibited chemotactic and signaling activities similar to that of free SDF-1 *in vitro*. In preparation for use in an animal wound model, the liposomes were allowed to infiltrate an acellular dermal scaffold, which occurred uniformly and in a timely manner. The positive outcomes of using the SDF-1 in vitro has led to the investigation of SDF-1 liposomes *in vivo*.

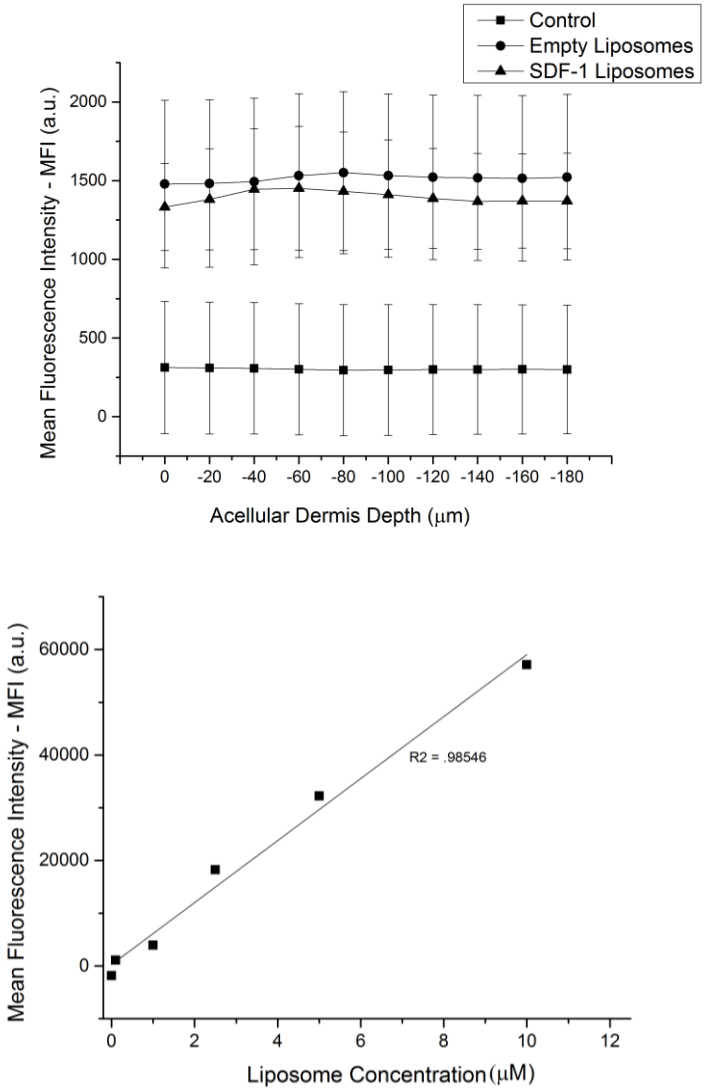

Figure 4.4. SDF-1 Liposomes Distributed in Acellular Dermis. (TOP) Acellular dermis punches (5mm ø) were incubated with PBS, 100µL of 1.13µM empty liposomes, or 100ng/mL SDF-1 bound to 1.13µM liposomes in 96-well plates. Liposomes were prelabeled with 1% DPPE-rhodamine. Optical slices at 5 locations per well were quantified and the average intensity is reported at increasing depths into the dermal scaffold. Acellular dermis thickness was ~200µm. N=4. (BOTTOM) Acellular dermis was loaded with increasing dilutions of the stock empty liposome suspension. Data shown are the fluorescence intensity as a function of phospholipid concentration. Representative curve from N=4 experiments.

4.5 REFERENCES

1 R. C. Fang, and R. D. Galiano, A Review of Becaplermin Gel in the Treatment of Diabetic Neuropathic Foot Ulcers, *Biologics,* 2 (2008), 1-12.

2 Schultz GS Chin GA, Chegini N, Diegelmann RF, 'Biochemistry of Wound Healing in Wound Care Practice', in *Wound Care Practice*, ed. by Paul SheffieldBest Publishing, Co., 2007).

3 J. J. Song, and H. C. Ott, Organ Engineering Based on Decellularized Matrix Scaffolds, *Trends Mol Med,* 17 (2011), 424-32.

4 S. Huang, and X. Fu, Naturally Derived Materials-Based Cell and Drug Delivery Systems in Skin Regeneration, *J Control Release,* 142 (2010), 149-59.

5 A. Sarkar, S. Tatlidede, S. S. Scherer, D. P. Orgill, and F. Berthiaume, Combination of Stromal Cell-Derived Factor-1 and Collagen-Glycosaminoglycan Scaffold Delays Contraction and Accelerates Reepithelialization of Dermal Wounds in Wild-Type Mice, *Wound Repair Regen,* 19 (2011), 71-9.

6 Q. Tan, H. Tang, J. Hu, Y. Hu, X. Zhou, Y. Tao, and Z. Wu, Controlled Release of Chitosan/Heparin Nanoparticle-Delivered Vegf Enhances Regeneration of Decellularized Tissue-Engineered Scaffolds, *Int J Nanomedicine,* 6 (2011), 929-42.

7 S. Guo, and L. A. Dipietro, Factors Affecting Wound Healing, *J Dent Res,* 89 (2010), 219-29.

8 D. Papakostas, F. Rancan, W. Sterry, U. Blume-Peytavi, and A. Vogt, Nanoparticles in Dermatology, *Archives of Dermatological Research,* 303 (2011), 533-50.

9 M. B. R. Pierre, and I. D. M. Costa, Liposomal Systems as Drug Delivery Vehicles for Dermal and Transdermal Applications, *Archives of Dermatological Research,* 303 (2011), 607-21.

10 F. Roesken, E. Uhl, S. B. Curri, M. D. Menger, and K. Messmer, Acceleration of Wound Healing by Topical Drug Delivery Via Liposomes, *Langenbecks Arch Surg,* 385 (2000), 42-9.

11 J. Wang, R. Wan, Y. Mo, M. Li, Q. Zhang, and S. Chien, Intracellular Delivery of Adenosine Triphosphate Enhanced Healing Process in Full-Thickness Skin Wounds in Diabetic Rabbits, *Am J Surg,* 199 (2010), 823-32.

12 J. Luo, Z. Luo, N. Zhou, J. W. Hall, and Z. Huang, Attachment of C-Terminus of Sdf-1 Enhances the Biological Activity of Its N-Terminal Peptide, *Biochem Biophys Res Commun,* 264 (1999), 42-7.

13 W. Hiesinger, J. M. Perez-Aguilar, P. Atluri, N. A. Marotta, J. R. Frederick, J. R. Fitzpatrick, 3rd, R. C. McCormick, J. R. Muenzer, E. C. Yang, R. D. Levit, L. J. Yuan, J. W. Macarthur, J. G. Saven, and Y. J. Woo, Computational Protein Design to Reengineer Stromal Cell-Derived Factor 1α Generates an Effective and Translatable Angiogenic Polypeptide Analog, *Circulation,* 124 (2011), S18-26.

14 A. Bandekar, S. Karve, M. Y. Chang, Q. Mu, J. Rotolo, and S. Sofou, Antitumor Efficacy Following the Intracellular and Interstitial Release of Liposomal Doxorubicin, *Biomaterials,* 33 (2012), 4345-52.

15 S. Sofou, J. L. Thomas, H. Y. Lin, M. R. McDevitt, D. A. Scheinberg, and G. Sgouros, Engineered Liposomes for Potential Alpha-Particle Therapy of Metastatic Cancer, *J Nucl Med,* 45 (2004), 253-60.

5. CHAPTER 5: SDF-1, sRAGE, AND SDF-1 LIPOSOMES DELIVERED IN DERMAL SCAFFOLDS IN AN IN VIVO DIABETIC MOUSE WOUND MODEL

Note: This chapter is partially reproduced from the following publication:

Przyborowski Olekson M, Faulknor R, Bandekar A, Sempkowski M, Hsia HC, Berthiaume F. Liposomally Enhanced Acellular Dermis for Diabetic Wound Healing. *Wound Repair and Regeneration (Submitted 05/2014).*

A. Bandekar and M. Sempkowski prepared liposomes for SDF-1 liposome in vivo treatments

5.1 INTRODUCTION

To test potential wound healing treatments, rodent models are favorable because they provide an *in vivo* environment where the quality of wound healing can be tracked over time. They are also cheap and provide reproducible results. In the following studies, excisional full-thickness wounds are created on genetically diabetic mice. The wound treatments are combined with acellular dermal scaffolds (either Alloderm® or Integra®) and wound image analysis is used to track closure. The treatments tested in this model include those previously discussed in chapters 3 and 4: SDF-1, SDF-1 liposomes, sRAGE, and sRAGE/SDF-1 combinations. The hypothesis is that the modifications to improve SDF-1 action (via sRAGE) and SDF-1 persistence (through liposomes) will improve wound healing *in vivo*.

There are many different types of diabetic rodent models in use to explore type 1 and type 2 diabetes and its complications. They are divided into two types: chemically induced and genetically modified. A common chemical used to induce diabetes is streptozotocin (STZ), which enters the β-islet cells in the pancreas and destroys them through the accumulation of free radicals. However, the STZ induction of diabetes (type 1 or 2) is highly dependent on dose and diet[1]. Genetically modified mice are also used; obesity and diabetes develop because of mutations in the leptin gene ($Lepr^{ob}$) or leptin

receptor ($Lepr^{db}$). The $Lepr^{ob}$ mouse becomes obese at 4 weeks and mildly hyperglycemic. The $Lepr^{db}$ mice also become obese at 4 weeks, but develop hyperglycemia between weeks 4-8, because of the failure of the pancreatic β-cells[1]. STZ-induced and genetically diabetic mice have been successfully used in wound healing[2, 3]. Since sRAGE has been previously used in the $Lepr^{db}$ diabetic model in a 2001 study by Goova, et al.[3], we utilized it in the following studies.

SDF-1 and sRAGE treatments have previously been tested on wounds. In our laboratory, the use of SDF-1 in combination with a dermal scaffold improved healing in wild type C57BL/6 mice. Not only did the wounds heal faster, but early inflammatory cell infiltrate was decreased while the amount of proliferating cells increased compared to the controls[4]. Only one publication has used SDF-1 in diabetic mice. SDF-1 and SDF-1 plus hyperbaric oxygen improved the healing of small 4-mm punch wounds in STZ-induced mice[5]. Therefore, treating larger wounds on genetically diabetic mice with SDF-1 and SDF-1 liposomes still needs to be explored. sRAGE has been used previously on $Lepr^{db}$ mice, where its application decreased inflammation, RAGE expression, and improved healing[3]. The combination of sRAGE plus SDF-1 or SDF-1 liposomes has not been previously tested.

In the following studies, various treatments were combined with dermal scaffolds in a $Lepr^{db}$ diabetic mouse excisional wound model. We first tested the effect of using free SDF-1 versus PBS and saw that SDF-1 alone was not effective in improving wound healing. We then used sRAGE to determine if that could improve healing of the free SDF-1. While we were able to reproduce the results found by Goova et al.[3], showing that sRAGE improved healing, the sRAGE + free SDF-1 combination was not significantly different then using free SDF-1 alone. We then tested the hypothesis that the hostile diabetic environment did not allow the SDF-1 to persist at the wound site by observing the difference between SDF-1 and SDF-1 Liposomes. The SDF-1 liposome treated

group significantly improved wound healing compared to free SDF-1 as shown by wound closure, persistent cell proliferation, and increased αSMA expression.

5.2 METHODS

5.2.1 Preparation of SDF-1 Liposomes

Liposomes were formed using previously published methods[6]. Briefly, 10μmol total lipid was combined in chloroform in a 25 mL round bottom flask at a mole ratio of 7:2:1 of DSPC:cholesterol:DSPA. For tracking, 1 mole % DPPE-rhodamine was added. All lipids were purchased from Avanti Polar Lipids. Chloroform was evaporated in a rotovapor for 10 minutes at 55°C followed by exposure to nitrogen for 5 minutes. The lipid film was hydrated in 1 mL of HEPES-sucrose buffer (pH = 7.4, Sigma-Aldrich) for 2 hours with final lipid concentration of 10 mM. The lipid suspension was extruded 21 times through two sizes of polycarbonate membranes, first with two stacked 200 nm pore size, and then with two stacked 100 nm pore size in an 80°C water bath. Liposomes were diluted to 100μM lipid and SDF-1 (R&D Systems) in HEPES-sucrose buffer was then added to the liposomes under vortexing at a molar ratio of 1:9 with respect to DSPA.

5.2.2 Diabetic Murine Excisional Wounding Surgery

All animal studies were carried out in accordance with National Research Council guidelines and were approved by the institutional animal care committee at Rutgers University. BKS.Cg-Dock7^{m}+/+Lepr(db)/J genetically diabetic mice were used at the age of 10 weeks (Jackson Laboratory, Bar Harbor, ME). One day prior to surgery, mice were anesthetized by isoflurane (Henry Schein) inhalation on a heating pad at 37°C. Anesthesia was deemed sufficient when the animal lacked a contracting reflex in response to a toe pinch. The eyes of the animal were covered with medical ointment (Henry Schein) to prevent dryness. Dorsal hair was clipped with remaining hair removed

using Nair™ cream (Church & Dwight Co). On the day of surgery, the mice were re-anesthetized, and the dorsum prepared by a three-fold alternating application of betadine scrub and 70% alcohol. A 1cm x 1cm square area was drawn with a black marker on the back of the animal using a template. The skin was gently lifted up and cut along the marked boundary to generate a full-thickness skin defect on the dorsum. An equivalent area of acellular dermal scaffold (Alloderm® [Life Cell] or Integra® [Integra Life Sciences]) was applied onto the wound, as described in table 5.1. The treatments in phases I and II were injected into the scaffold after it was placed on the wound. sRAGE was provided by the Schmidt laboratory at NYU. The treatments in phase III were presoaked onto the dermal scaffold. In all cases, the wound was covered by Tegaderm™ (3M), a semi-occlusive silicone dressing, and secured with 6-0 black silk braided sutures. Gross wound morphology was monitored over 35 days and digital images of the wounds were taken weekly. Wound area was quantified by tracing the wound in ImageJ. The wound closure percentage was calculated using the formula: (1-remaining open wound area/initial wound area) x 100. N=5-7 animals per group.

Phase	I	II	III
Skin Substitute	Integra®	Integra®	Alloderm®
Treatments	-1μg SDF-1 in 100 μL PBS on day 0 -100 μL PBS on day 0	-20μg sRAGE in 100 μL PBS on days 0, 2, 4, and 6 -1μg SDF-1 in 100 μL PBS on day 0 + 20μg sRAGE in 100 μL PBS on days 0, 2, 4, and 6	-1μg SDF-1 in 100 μL PBS on day 0 -100 μL PBS on day 0 -Liposomes containing 0.88μg SDF-1 in 100μL PBS -Liposomes in 100μL PBS

Table 5.1 *In vivo* diabetic wound treatments

5.2.3 Wound Tissue Analysis and Histology

On postwounding days 7, 21, and 28, animals were sacrificed and wounds excised. Half of the tissues were processed for protein analysis while the other half were

fixed for histology. For protein assays, tissue pieces were homogenized in RIPA buffer with 1:100 EDTA and 1:100 Halt protease inhibitor cocktail (ThermoFisher Scientific). Tissue suspensions were rotated for 2 hours at 4°C and then centrifuged for 20 minutes at 16,000 x g at 4°C. BCA was performed to determine total protein content (ThermoFisher Scientific). A western blot was performed to measure αSMA content using 10% SDS-PAGE gel electrophoresis (BIO-RAD). Equal amounts of protein were placed in each lane of the gel and subsequently transferred to nitrocellulose membranes. Non-specific binding was blocked by a 2-hour incubation at room temperature with 5% non-fat dry milk in Tris-buffered saline containing 0.1% Tween-20 (TBST) (BIO-RAD). Primary rabbit polyclonal αSMA antibody was incubated with the membrane for 16 hours at 4°C in the blocking solution (Abcam). After incubation, membranes were washed with TBST and then incubated for 1 hour with a secondary antibody goat anti-rabbit IgG HRP (Abcam) at room temperature. Membranes were washed in TBST and binding sites were identified by SuperSignal™ west picochemiluminescent assay (ThermoFisher Scientific) for 5 minutes. Bands were digitized with a scanner.

For histology, wound tissues were fixed in 10% formalin (VWR) for 24 hours and then stored in ethanol at 4°C. Tissues were then paraffin embedded and thin sections stained with hematoxylin and eosin (H&E) to visualize tissue morphology, or picosirius red (Direct Red 80 mixed with picric acid) to visualize collagen deposition. Immunohistochemistry was performed with αSMA rabbit monoclonal (Epitomics) and Ki67 proliferation antigen (Lab Vision) rabbit monoclonal antibodies.

5.2.4 Statistics

All values are presented as means ± standard error of the mean (SEM). Multiple comparisons were carried out using one-way ANOVA followed by post-hoc analysis. Post-hoc tests are indicated in the figure legends.

5.3 RESULTS AND DISCUSSION

5.3.1 Phase I: Free SDF-1 Effectiveness In Vivo

Free SDF-1 was added to the Integra® dermal scaffold in diabetic excisional mouse wounds and compared to the PBS buffer control (Table 5.2). Unlike normal mice, where SDF-1 improved healing significantly over buffer[4], free SDF-1 treatment in diabetic mice did not improve healing. Instead, SDF-1 treated wounds healed slower than buffer treated wounds, though the difference was not significant. We hypothesized that the decrease in SDF-1 effectiveness was due to the diabetic environment that exists in the $Lepr^{db}$ mice, which has previously been characterized by increased inflammation and MMP levels[3].

	Treatment	
Day	PBS	Free SDF-1
7	6.9 ± 12.3	14.0 ± 17.3
14	39.8 ± 15.4	41.8 ± 13.5
21	84.3 ± 6.6	69.2 ± 10.5
28	90.3 ± 5.0	82.0 ± 7.3

Table 5.2 Phase I Results: Free SDF-1. Integra® dermal scaffold with stated treatment was applied to a 1cm^2 excisional wound at day 0. Data shown represent the percent fraction of original open wound area that is now filled with tissue. N=7.

5.3.2 Phase II: sRAGE and sRAGE/SDF-1 Combination Effectiveness In Vivo

Given the ineffectiveness of free SDF-1 in improving wound healing in the mouse model, we explored using the sRAGE strategy that improved SDF-1 function in the HL-60 cell *in vitro* studies. As shown in table 5.3, sRAGE was tested alone and in combination with SDF-1. Compared to free SDF-1, sRAGE treatment alone showed a

significant increase in fractional wound closure at day 28. While the sRAGE + SDF-1 combination showed a similar change compared to free sRAGE, the difference was not significant. The application of sRAGE only addresses some aspects of the diabetic wound environment and may restore signaling, but may not prevent proteolytic degradation. Another limitation of the combination treatment is no exploration of the timing of treatments; the SDF-1 was applied on day 0 and sRAGE was applied on days 0, 2, 4, and 6. Therefore, future studies can explore this timing, where we hypothesize that the most effective combination would be early treatment of sRAGE to decrease the inflammation, followed by a period of SDF-1 treatment to improve cellular migration and proliferation, since SDF-1 production is higher at the wound margins in the proliferation phase compared to the inflammatory phase[7, 8]. In addition, the SDF-1 liposome delivery system is explored *in vivo* and can be used in combination with sRAGE treatment.

	Treatment		
Day	Free sRAGE	Free SDF-1 + Free sRAGE	Free SDF-1
7	-3 ± 14.4	17.7 ± 7.9	14.0 ± 17.3
14	44.8 ± 12.0	50.7 ± 10.4	41.8 ± 13.5
21	85.2 ± 5.5	82.0 ± 6.7	69.2 ± 10.5
28	99.6 ± 0.4**	91.7 ± 5.4	82.0 ± 7.3

Table 5.3 Phase II Results: Free sRAGE alone and in combination with SDF-1. Integra® dermal scaffold with stated treatment was applied to a 1cm^2 excisional wound at day 0. Data shown represent the percent fraction of original open wound area that is now filled with tissue. Free sRAGE and Free SDF-1 + Free sRAGE N=5. SDF-1 N=7. **: value for sRAGE is significantly higher than free SDF-1 group at day 28 ($p < 0.05$, one way ANOVA, Fisher's LSD post-test).

5.3.3 Phase III: SDF-1 Liposome Effectiveness In Vivo

For phase III, Alloderm® was loaded with either SDF-1 liposomes or an approximately similar amount of free SDF-1 (table 5.4). Using wound closure as the metric, free SDF-1 did not improve the wound closure rate compared to the baseline response with PBS treatment, as in both cases, wounds closed at around post wounding day 28; this finding in Alloderm® was consistent with the previous studies of free SDF-1 versus PBS in Integra®. In contrast, wounds covered with Alloderm® containing SDF-1 liposomes were nearly all closed at postwounding day 21, which was reflected in a ~15% greater fractional closure compared to all other groups at that time. All other groups eventually closed their wounds, albeit one week later. Empty liposomes did not significantly accelerate wound closure, indicating that the presence of SDF-1 was required to have a significant impact on the wound healing process.

	Treatments			
Day	PBS	Empty Liposomes	Free SDF-1	SDF-1 Liposomes
7	-5.8 ± 7.4	-28.3 ± 14.4	-9.0 ± 11.0	-3.0 ± 6.6
14	46.1 ± 7.1	44.8 ± 9.0	34.5 ± 11.9	51.9 ± 12.6
21	72.7 ± 8.6	78.2 ± 5.1	72.9 ± 4.9	93.0 ± 3.2
28	93.4 ± 3.0	93.3 ± 3.1	86.5 ± 5.3	97.0 ± 3.0

Table 5.4 Phase III Results: SDF-1 Liposomes. Alloderm® with stated treatment was applied to a 1cm^2 excisional wound at day 0. Data shown represent the percent fraction of original open wound area that is now filled with tissue. N=5.: value for SDF-1 liposomes is significantly higher than other groups at day 21 ($p < 0.05$, one way ANOVA, Fisher's LSD post-test).**

Although the empty liposome condition appears to increase wound area at day 7, this difference was not statistically significant.

SDF-1 liposomes reduced the wound closure time by one whole week compared to free SDF-1 in a diabetic mouse skin excision wound model. Interestingly, free SDF-1 provided no benefit with respect to wound closure rate compared to free liposomes or plain buffer. It is noteworthy that the dosage and schedule of SDF-1 administration used shown here (a single 1μg application) was lower to that used in a prior publication in wild-type mice, which used 4 doses of 1μg each of free SDF-1 on the first 4 days after wounding[4]. It is possible that the lack of an effect of free SDF-1 here is due to the lower overall dose and/or the difference in animal model. Diabetic mice heal significantly slower than their wild-type counterparts, and therefore may especially benefit from more prolonged growth factor stimulation.

5.3.4 Histology and Protein Analysis

We then probed the mechanism of action of the SDF-1 liposomes using histological staining and western blotting. On day 7 post-wounding, the H&E stained cross sections the accumulation of inflammatory infiltrates in all groups (figure 5.1A), with no observable differences among the groups. At later time points, the infiltrate decreased in all cases, and fully closed wounds had a scarred area with thick granulation tissue. When granulation tissue was scored on a published histological scale[3], sections of SDF-1 liposome treated tissue scored significantly higher at day 21 than the buffer and empty liposome treated groups and at day 28 than the empty liposome treated group (figure 5.1B). Wounds treated with free SDF-1 and SDF-1 liposomes showed more widespread expression of the Ki67 proliferation antigen within the open wound area at day 7 compared to the other groups (figure 5.2A). Ki67 expression decreased by day 21 for all groups, and proliferation remained present in keratinocytes in the basal layer of the

epidermis (figure 5.2B, yellow arrows). In addition, at this point, proliferation was clearly the highest in the SDF-1 liposome group, which exhibited nest-like regions of Ki67 positive cells in the dermis, (figure 5.2B, red arrows); the organization of these cells around a lumen suggests they are endothelial (figure 5.2B, inset). While the buffer control and empty liposome groups exhibited some remaining Ki67 expression in the epidermis, there was virtually none in the dermis. On post-wounding day 28, some Ki67 stain remained in the keratinocyte basal layer (figure 5.2C, yellow arrows); however, while the dermis of wounds treated with SDF-1 liposomes retained proliferation in resident cells (fibroblasts, endothelial cells), it had ceased in all the other treatment groups (figure 5.2C, red arrows). Quantification of the proliferation at day 7 confirmed higher area of percent positive Ki67 cells in the free SDF-1 and SDF-1 liposome groups (figure 5.2D).

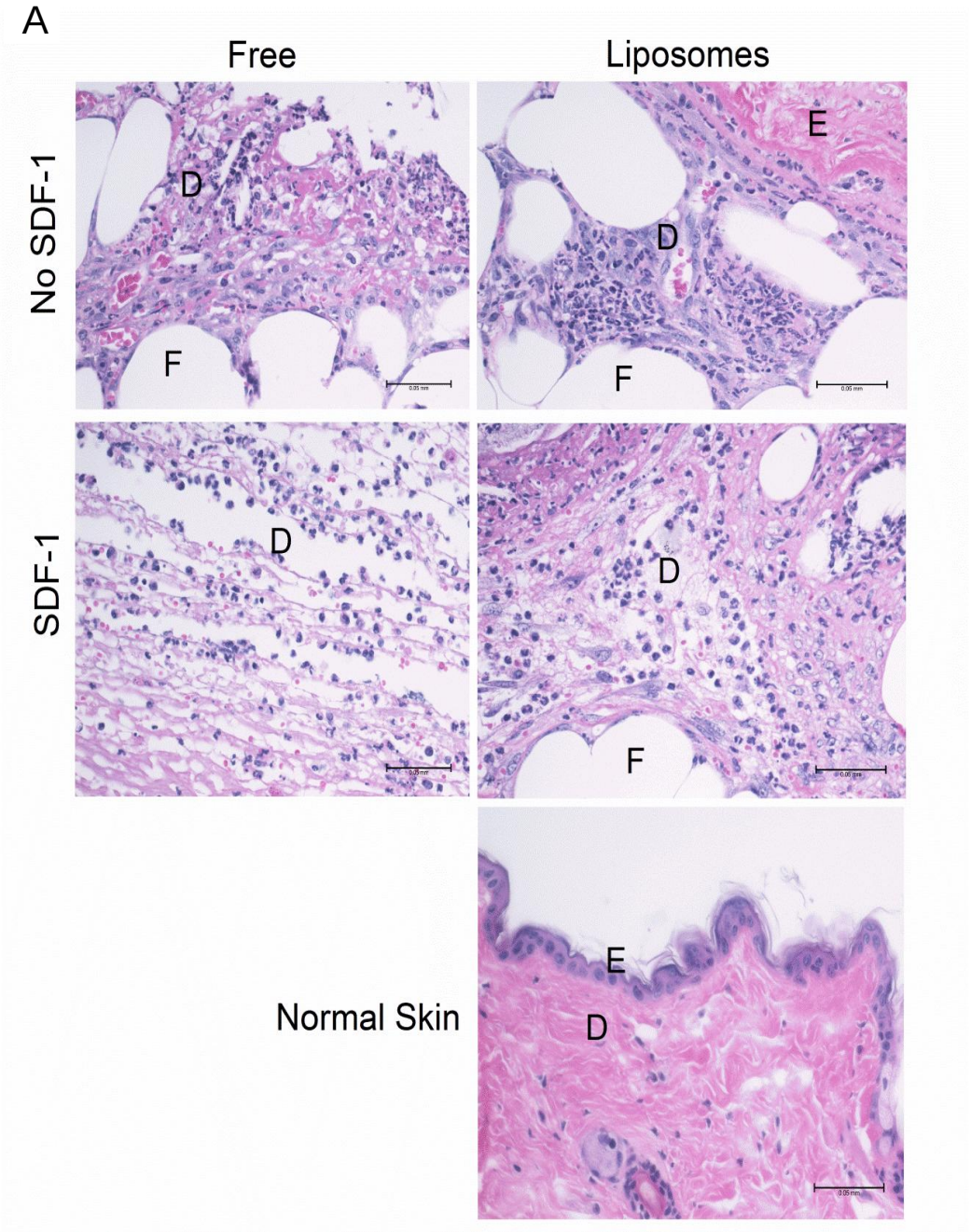
A
Free
Liposomes
No SDF-1
SDF-1
Normal Skin
D
F
E
D
F
D
D
F
E
D

B

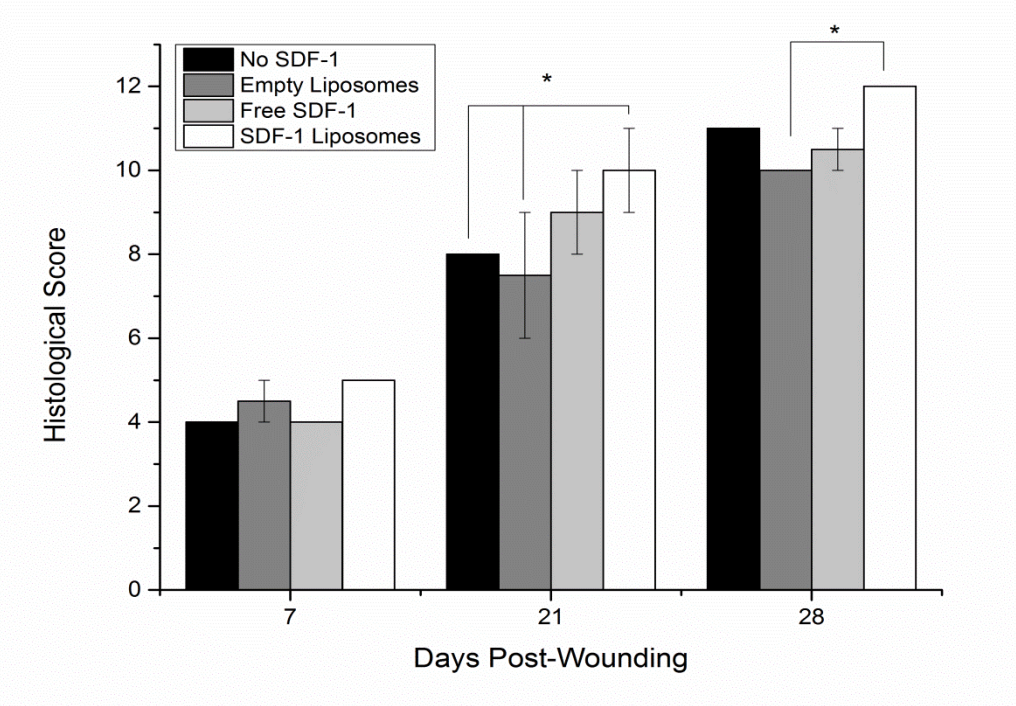

Figure 5.1 H&E Stain of Phase III Treated Tissue. Wound tissues were harvested 7 days after wound creation. (A) Images shown are H&E stained tissue sections in paraffin visualized at 40x magnification (purple = cell nuclei, pink = cytoplasm and collagen). Wound structures are labeled as: (E) Epidermis (D) Dermis (F) Fat. Representative images from N=2 animals. Scale bar = 50μm (B) Histological scoring based on previous literature[3]. In brief, score of 1-3: minimal cell accumulation, granulation tissue, or epithelial cells; 4-6: immature granulation tissue, mostly inflammatory cells, a few fibroblasts, a few capillaries, minimal collagen, minimal epithelialization; 7-9: moderate granulation tissue thickness, more domination of fibroblasts and epithelial cells, neovascularization; 10-12: thick, vascularized granulation tissue, mostly fibroblasts, extensive collagen, partial to complete coverage of wound by epithelial cells. N=2 *: value for SDF-1 liposomes is significantly higher than buffer and empty liposome treated groups at day 21 and empty liposome group at day 28 ($p < 0.05$, one way ANOVA, Fisher's LSD post-test).

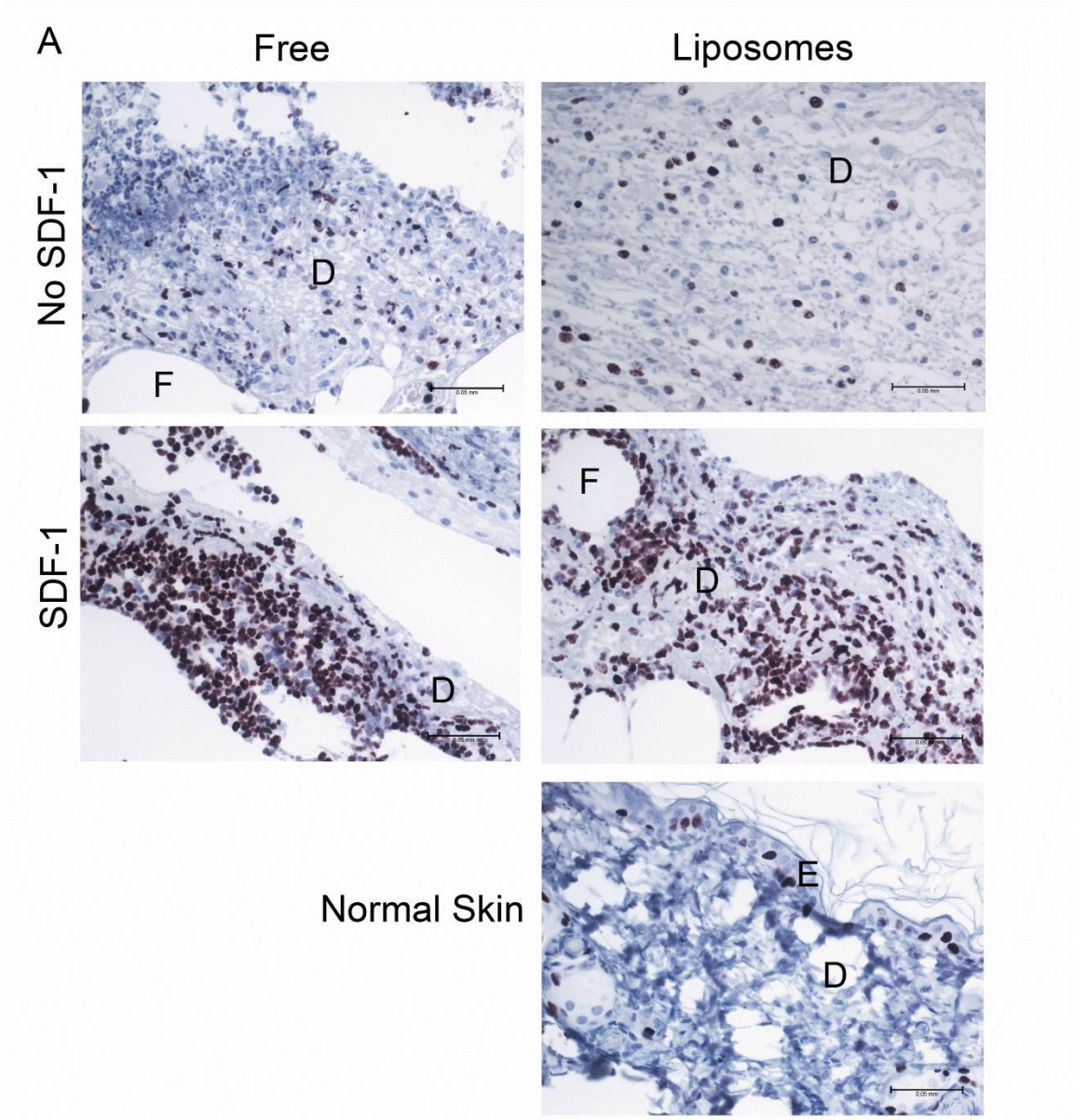
A
Free
Liposomes
No SDF-1
SDF-1
Normal Skin
D
F
D
F
D
E
D

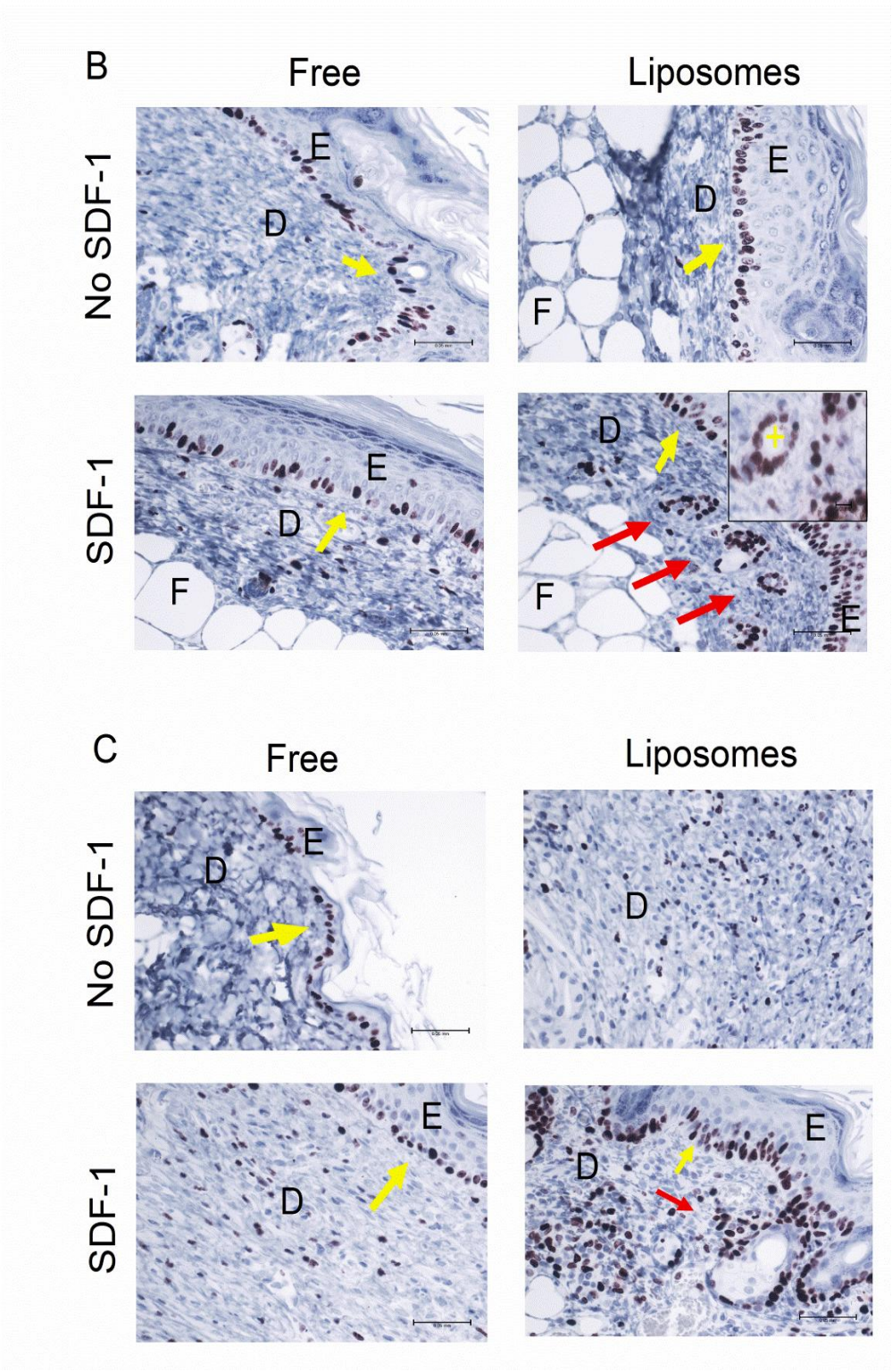
B
Free
Liposomes
No SDF-1
SDF-1
E
D
F
C
Free
Liposomes
No SDF-1
SDF-1
E
D

D

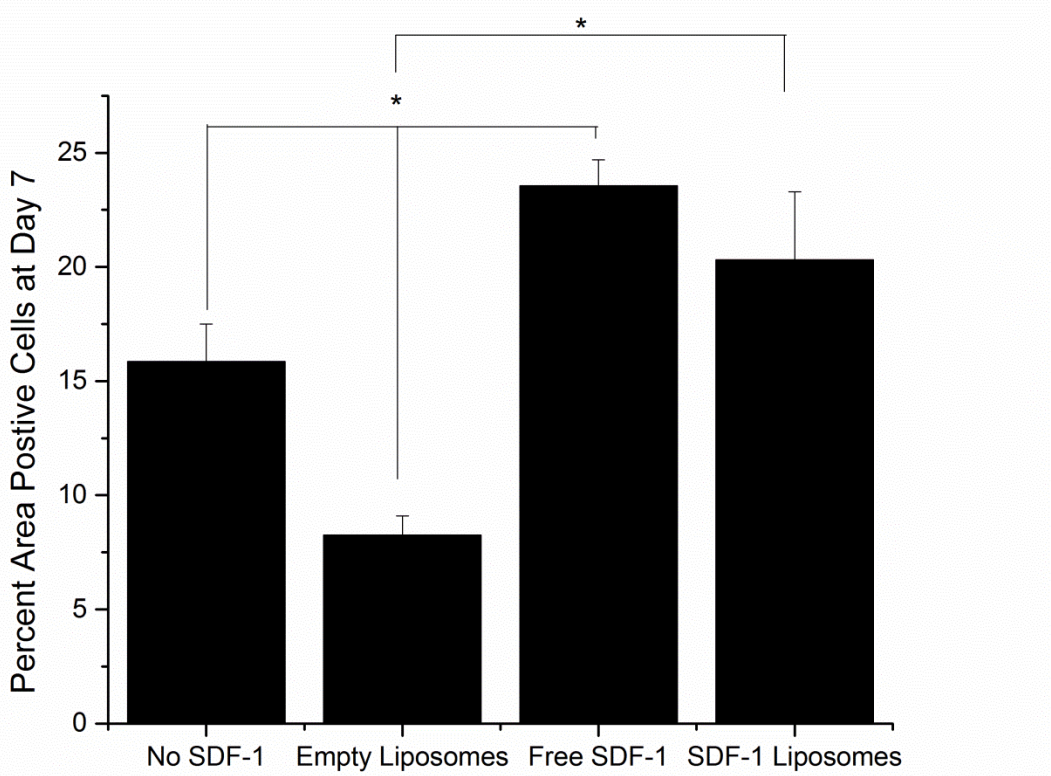

Figure 5.2 Ki67 Stain of Phase III Treated Tissue. Wound tissues were harvested 7, 21, and 28 days after wound creation, sectioned and stained for Ki67, and visualized with a 40x objective (brown = proliferating cells). Representative images are shown for (A) day 7, (B) day 21, and (C) day 28. Wound structures are labeled as: (E) Epidermis (D) Dermis (F) Fat. Yellow arrows represent proliferating basal keratinocytes. Red arrows represent clusters of proliferating cells in the dermis. Inset in (B) represents 100x image of these cells, where they are proliferating around a lumen space (plus sign). Representative images from N=2 animals. Scale bar = 50μm. (D) Percent area of positive Ki67 cells at day 7. N=2 *: value for free SDF-1 is significantly higher than buffer and empty liposome treated groups; value for SDF-1 liposomes is significantly higher than empty liposomes ($p < 0.05$, one way ANOVA, Fisher's LSD post-test).

We observed that Ki67 expression in the dermis was significantly more sustained in the wounds treated with SDF-1 liposomes compared with free SDF-1. The difference was especially striking at days 21 and 28 post wounding, where most of the dissimilarity in wound closure rate was observed. These results suggest that the liposome system enables prolonged delivery of SDF-1 to the wound, with a single application of the SDF-1 liposome having effects lasting as much as 4 weeks. The target of SDF-1 in the wound appears to be mostly fibroblasts and endothelial cells which are necessary to build granulation tissue[9]. Both cell types have been identified as CXCR4 expressing cells via flow cytometry and PCR, and there is evidence in literature that fibroblasts[10] and endothelial cells[11] migrate in response to SDF-1.

Next we examined the expression of αSMA, which is a marker of myofibroblasts, the main cell type implicated in wound contraction, a key process for wound closure[9]. Expression of αSMA was not apparent histochemically at day 7, and started to appear at day 21, although the staining was still faint (figure 5.3). By day 28, αSMA levels were higher in the SDF-1 and SDF-1 liposome conditions compared to the other groups. Immunoblotting for αSMA showed that, at day 7, the SDF-1 and SDF-1 liposome groups had the least expression of αSMA, while by day 28, they expressed more αSMA compared to the control buffer and empty liposome groups (figure 5.4). The altered dynamics of myofibroblasts, which are known to secrete collagen at high rates[12], did not however translate into differences in the collagen fiber arrangement at day 28. Picosirius Red, which colors collagen green and progressively yellow, orange, and red as fiber thickness increases[13], revealed thick red collagen fibers comparable to normal skin at day 28, with no differences in color among the groups (figure 5.5A). Percent collagen area was significantly higher in the SDF-1 liposome group than the buffer and empty liposome treated groups (figure 5.5B).

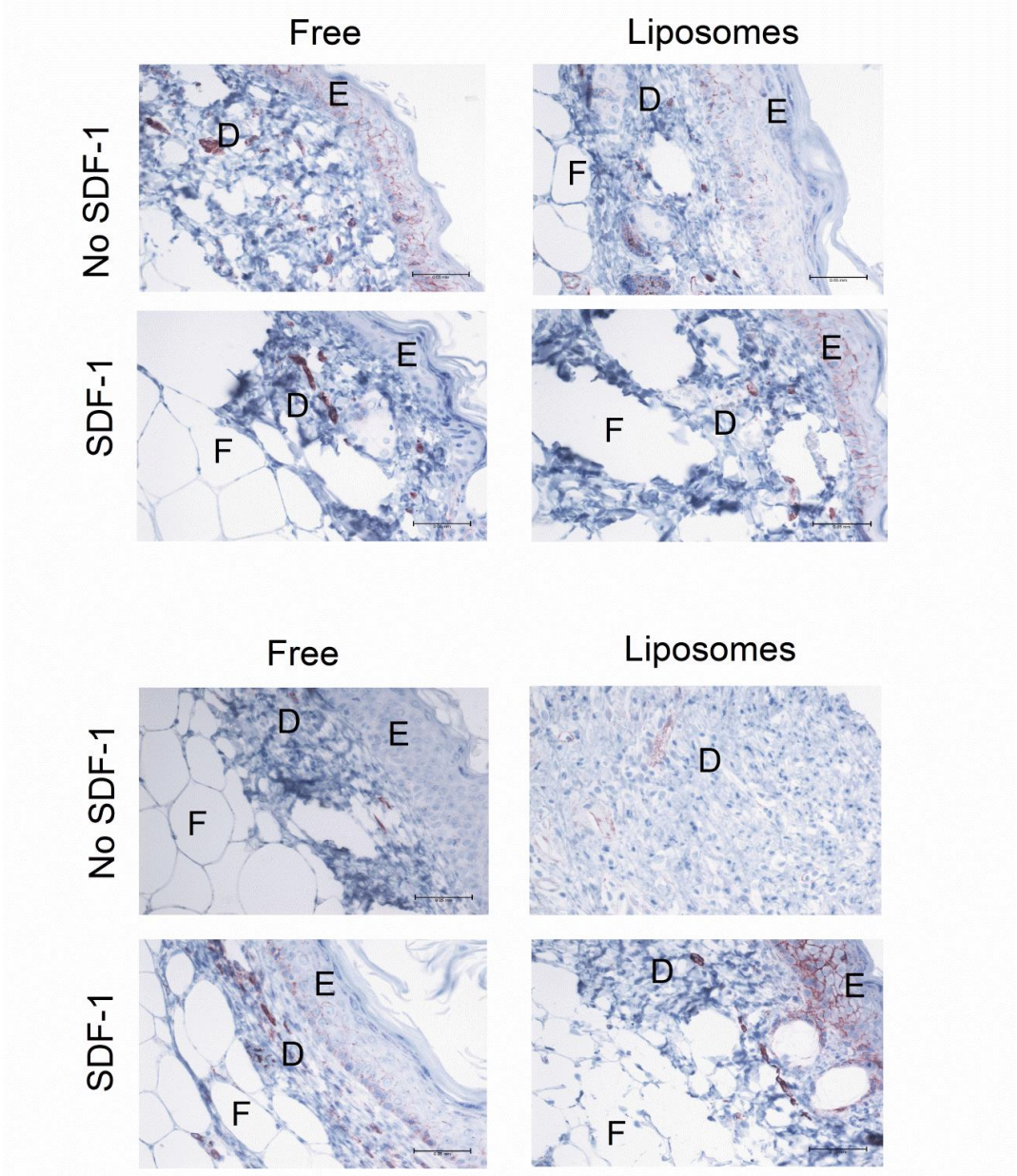

Figure 5.3 αSMA stained Phase III Treated Tissue. Wound tissues were harvested 21, and 28 days after wound creation, sectioned and stained for αSMA, and visualized with a 40x objective (brown = positive for αSMA). Representative images are shown for (TOP) day 21, and (BOTTOM) day 28. Wound structures are labeled as: (E) Epidermis (D) Dermis (F) Fat. Representative images from N=2 animals. Scale bar = 50μm.

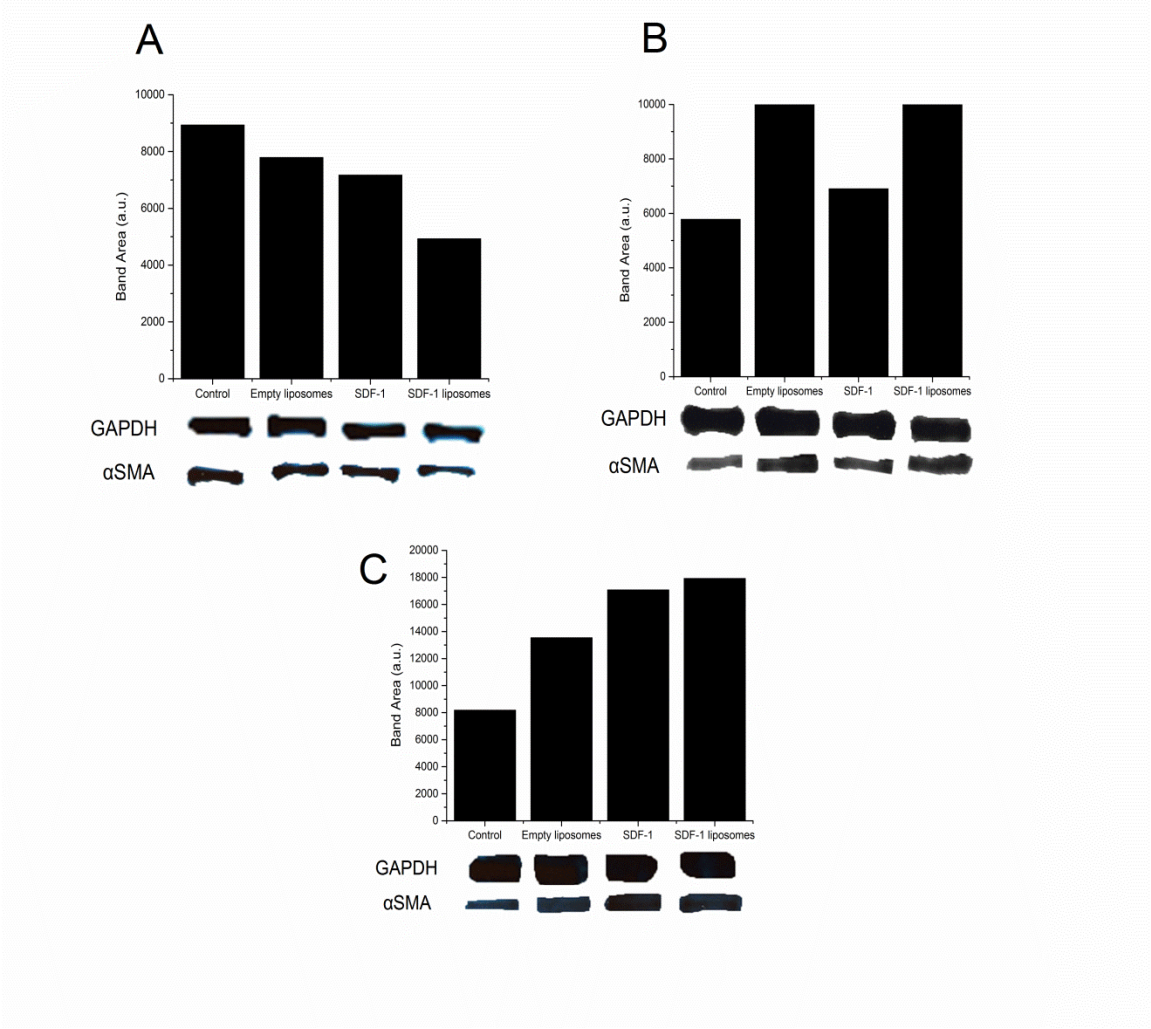

Figure 5.4 αSMA Western Blot for Phase III Treated Tissue. Wound tissues were harvested 7, 21, and 28 days after wound creation, and processed for immunoblotting for αSMA. Representative bands from N=2 animals and densitometry by ImageJ are shown for each condition at (A) day 7, (B) day 21, and (C) day 28. GAPDH was used as internal loading control.

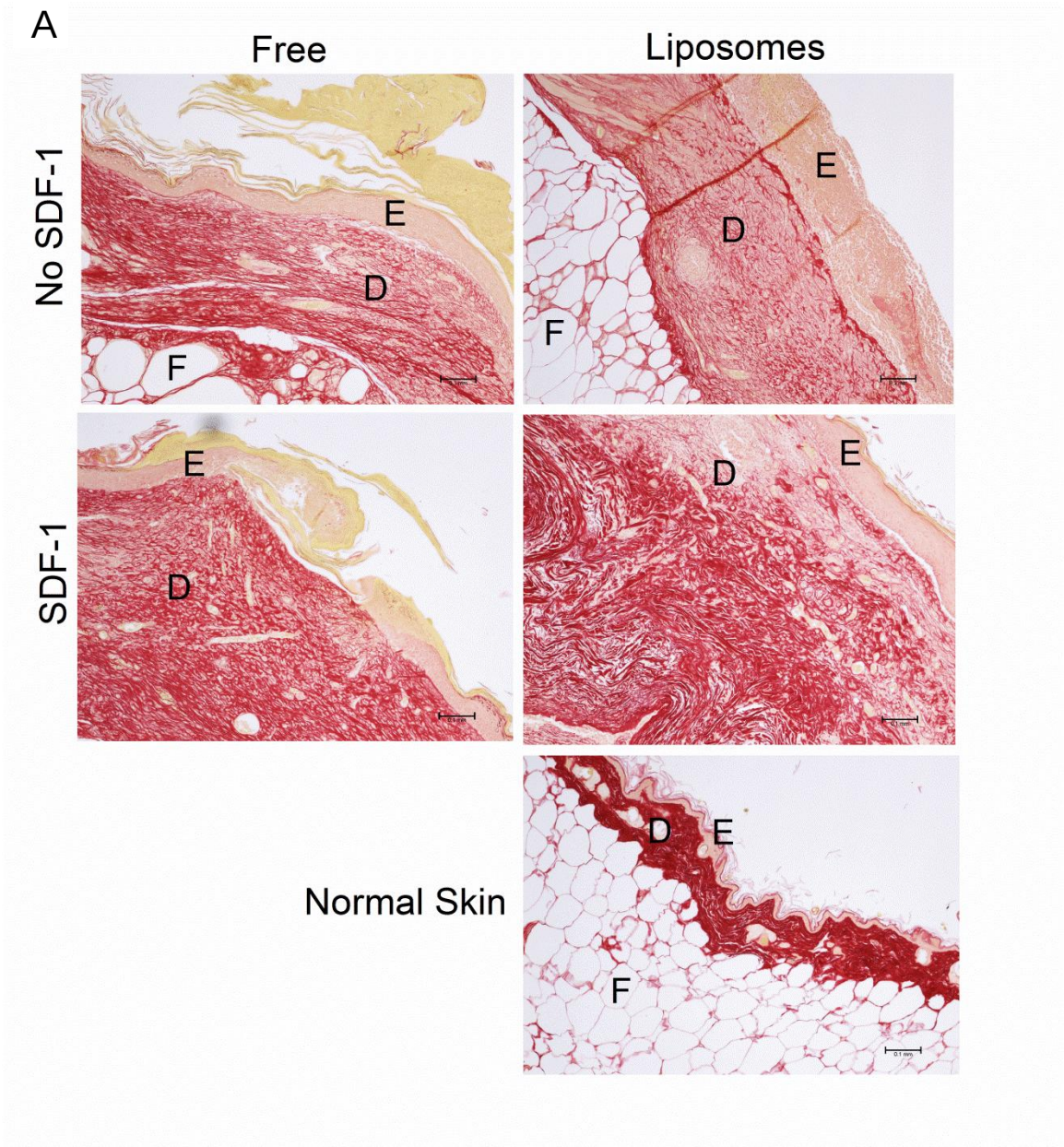
A
Free
Liposomes
No SDF-1
SDF-1
Normal Skin
E
D
F

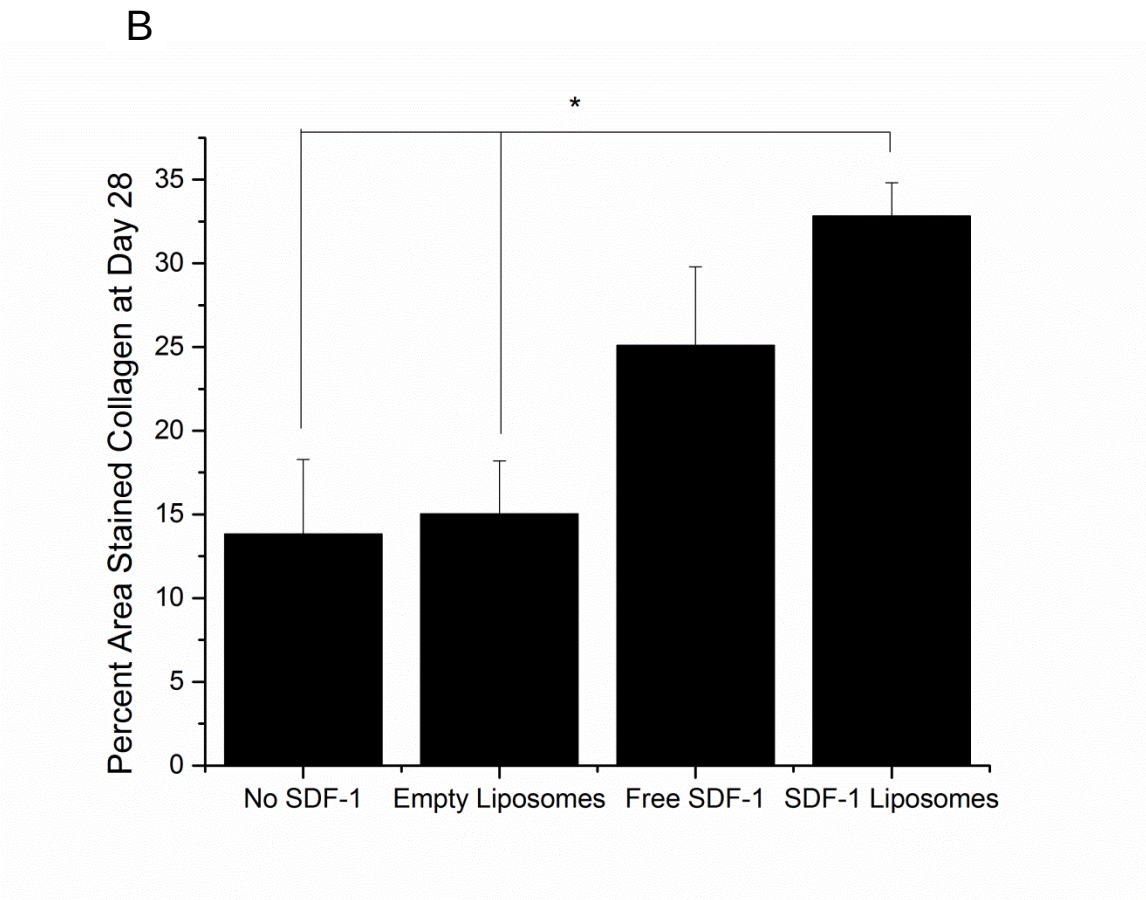

Figure 5.5 Picosirius Red Stain for Phase III Treated Tissue. Wound tissues were harvested 28 days after wound creation, sectioned and stained for collagen using picosirius red, and visualized with a 10x objective (red = collagen). Representative images are shown. Wound structures are labeled as: (E) Epidermis (D) Dermis (F) Fat. Scarred tissue area is much thicker with a less organized structure (lighter red shade of staining) than normal skin. Representative images from N=2 animals. Scale bar = 100μm. (D) Percent area of stained collagen at day 28. N=2 *: value for SDF-1 liposomes is significantly higher than buffer and empty liposome treated groups ($p < 0.05$, one way ANOVA, Fisher's LSD post-test).

The persistence of the SDF-1-mediated dermal proliferation and ultimately faster wound closure achieved with the SDF-1 liposomes may reflect longer persistence of SDF-1 in the wound. Wound fluid contains proteases that break down SDF-1, and it is plausible that this process is mitigated in the liposome configuration. Prior studies have shown that negatively charged heparin sulfate binds SDF-1 and induces SDF-1 dimerization[14, 15]. This dimerization was found to inhibit its proteolysis; for example, dipeptidyl peptidase IV (DPP IV)-mediated breakdown of free SDF-1 was significantly inhibited in the presence of heparin sulfate, which blocks the DPP IV cleavage site located on the N-terminal side[16]. However, dimerization was also found to inhibit biological activity, and it is therefore surprising that this inhibition was not observed with the SDF-1 liposomes. It is also possible that the liposome configuration enhances penetration through tissue since liposome systems have been shown to be effective transdermal delivery systems[17], and the efficacy of liposomal forms of drugs often exceeds that of the free compound in skin wounds[18-20].

5.4 CONCLUSION

To improve growth factor treatments in diabetic wounds, SDF-1 was used as a treatment in combination with sRAGE and within a liposome delivery system. Though the use of the sRAGE/SDF-1 combination did not show a significant difference, sRAGE alone improved wound closure, which is consistent with prior literature. We hypothesized that the SDF-1 treatment was being degraded by MMPs which are upregulated in diabetic wounds. Therefore, an SDF-1 liposome delivery system was created, so that the SDF-1 can persist at the wound site. The used of SDF-1 liposomes increased the fractional area of closed tissue by at least 15% over the other groups at day 21. This difference was likely due to an increase in dermal cell proliferation and myofibroblast aided contraction. While future studies look to combine the sRAGE treatment with the

SDF-1 liposomes, the current SDF-1 liposome platform described herein could in principle be easily modified to included different peptides and be incorporated into any type of dermal scaffold; the typical pore size of such materials is on the order of 10 µm or more, which is 2 orders of magnitude larger than the typical size of the SDF-1 liposomes. The modular treatment could also be expanded for use in other applications using decellularized matrices, as the SDF-1 can be exchanged for other positively charged factors and the Alloderm® can be replaced with other matrices.

5.5 REFERENCES

1 A. Chatzigeorgiou, A. Halapas, K. Kalafatakis, and E. Kamper, The Use of Animal Models in the Study of Diabetes Mellitus, *In Vivo,* 23 (2009), 245-58.

2 N. Ruzehaji, Z. Kopecki, E. Melville, S. L. Appleby, C. S. Bonder, R. M. Arkell, R. Fitridge, and A. J. Cowin, Attenuation of Flightless I Improves Wound Healing and Enhances Angiogenesis in a Murine Model of Type 1 Diabetes, *Diabetologia,* 57 (2014), 402-12.

3 M. T. Goova, J. Li, T. Kislinger, W. Qu, Y. Lu, L. G. Bucciarelli, S. Nowygrod, B. M. Wolf, X. Caliste, S. F. Yan, D. M. Stern, and A. M. Schmidt, Blockade of Receptor for Advanced Glycation End-Products Restores Effective Wound Healing in Diabetic Mice, *Am J Pathol,* 159 (2001), 513-25.

4 A. Sarkar, S. Tatlidede, S. S. Scherer, D. P. Orgill, and F. Berthiaume, Combination of Stromal Cell-Derived Factor-1 and Collagen-Glycosaminoglycan Scaffold Delays Contraction and Accelerates Reepithelialization of Dermal Wounds in Wild-Type Mice, *Wound Repair Regen,* 19 (2011), 71-9.

5 K. A. Gallagher, Z. J. Liu, M. Xiao, H. Chen, L. J. Goldstein, D. G. Buerk, A. Nedeau, S. R. Thom, and O. C. Velazquez, Diabetic Impairments in No-Mediated Endothelial Progenitor Cell Mobilization and Homing Are Reversed by Hyperoxia and Sdf-1 Alpha, *J Clin Invest,* 117 (2007), 1249-59.

6 A. Bandekar, S. Karve, M. Y. Chang, Q. Mu, J. Rotolo, and S. Sofou, Antitumor Efficacy Following the Intracellular and Interstitial Release of Liposomal Doxorubicin, *Biomaterials,* 33 (2012), 4345-52.

7 T. E. Restivo, K. A. Mace, A. H. Harken, and D. M. Young, Application of the Chemokine Cxcl12 Expression Plasmid Restores Wound Healing to near Normal in a Diabetic Mouse Model, *J Trauma,* 69 (2010), 392-8.

8 A. Toksoy, V. Muller, R. Gillitzer, and M. Goebeler, Biphasic Expression of Stromal Cell-Derived Factor-1 During Human Wound Healing, *Br J Dermatol,* 157 (2007), 1148-54.

9 L. Macri, and R. A. Clark, Tissue Engineering for Cutaneous Wounds: Selecting the Proper Time and Space for Growth Factors, Cells and the Extracellular Matrix, *Skin Pharmacol Physiol,* 22 (2009), 83-93.

10 Y. Yang, S. K. Shim, H. A. Kim, M. Seon, E. Yang, D. Cho, and S. I. Bang, Cxc Chemokine Receptor 4 Is Essential for Lipo-Pge1-Enhanced Migration of Human Dermal Fibroblasts, *Exp Dermatol,* 21 (2012), 75-7.

11 J. Yamaguchi, K. F. Kusano, O. Masuo, A. Kawamoto, M. Silver, S. Murasawa, M. Bosch-Marce, H. Masuda, D. W. Losordo, J. M. Isner, and T. Asahara, Stromal Cell-Derived Factor-1 Effects on Ex Vivo Expanded Endothelial Progenitor Cell Recruitment for Ischemic Neovascularization, *Circulation,* 107 (2003), 1322-8.

12 J. P. Cleutjens, M. J. Verluyten, J. F. Smiths, and M. J. Daemen, Collagen Remodeling after Myocardial Infarction in the Rat Heart, *Am J Pathol,* 147 (1995), 325-38.

13 L. Rich, and P. Whittaker, Collagen and Picosirius Red Staining: A Polarized Light Assessment of Fibrillar Hue and Spatial Distribution, *Braz J Morphol Sci,* 22 (2005), 97-104.

14 R. Sadir, A. Imberty, F. Baleux, and H. Lortat-Jacob, Heparan Sulfate/Heparin Oligosaccharides Protect Stromal Cell-Derived Factor-1 (Sdf-1)/Cxcl12 against

Proteolysis Induced by Cd26/Dipeptidyl Peptidase Iv, *J Biol Chem,* 279 (2004), 43854-60.

15 C. L. Salanga, and T. M. Handel, Chemokine Oligomerization and Interactions with Receptors and Glycosaminoglycans: The Role of Structural Dynamics in Function, *Exp Cell Res,* 317 (2011), 590-601.

16 J. J. Ziarek, C. T. Veldkamp, F. Zhang, N. J. Murray, G. A. Kartz, X. Liang, J. Su, J. E. Baker, R. J. Linhardt, and B. F. Volkman, Heparin Oligosaccharides Inhibit Chemokine (Cxc Motif) Ligand 12 (Cxcl12) Cardioprotection by Binding Orthogonal to the Dimerization Interface, Promoting Oligomerization, and Competing with the Chemokine (Cxc Motif) Receptor 4 (Cxcr4) N Terminus, *J Biol Chem,* 288 (2013), 737-46.

17 M. B. R. Pierre, and I. D. M. Costa, Liposomal Systems as Drug Delivery Vehicles for Dermal and Transdermal Applications, *Archives of Dermatological Research,* 303 (2011), 607-21.

18 D. Papakostas, F. Rancan, W. Sterry, U. Blume-Peytavi, and A. Vogt, Nanoparticles in Dermatology, *Archives of Dermatological Research,* 303 (2011), 533-50.

19 F. Roesken, E. Uhl, S. B. Curri, M. D. Menger, and K. Messmer, Acceleration of Wound Healing by Topical Drug Delivery Via Liposomes, *Langenbecks Arch Surg,* 385 (2000), 42-9.

20 J. Wang, R. Wan, Y. Mo, M. Li, Q. Zhang, and S. Chien, Intracellular Delivery of Adenosine Triphosphate Enhanced Healing Process in Full-Thickness Skin Wounds in Diabetic Rabbits, *Am J Surg,* 199 (2010), 823-32.

6. CHAPTER 6: CONCLUSION

6.1 KEY FINDINGS

6.1.1 Summary of Dissertation Findings

The goal of this dissertation was to improve SDF-1 function by blocking the pro-inflammatory environment with sRAGE and by packing the SDF-1 into liposomes. We found that sRAGE improved SDF-1 directed migration in an *in vitro* high glucose culture through restoration of superoxide levels. When sRAGE was added to an *in vivo* wound model, it improved wound healing significantly over free SDF-1. Prepared SDF-1 liposomes maintained SDF-1 function *in vitro* and improved healing *in vivo* through increased cell proliferation and promotion of wound contraction.

6.1.2 sRAGE Improves SDF-1 Directed Migration in an In Vitro High Glucose Culture through Restoration of Superoxide levels

To determine the effectiveness of sRAGE at improving SDF-1 directed migration, we had to first develop a transwell migration assay. Using prior literature, the transwell migration assay was setup to measure SDF-1 directed cell migration of HL-60 cells. As the dose of SDF-1 increased, migration increased, showing a correlation between SDF-1 amount and migratory function. When glucose was added into the media as a 24-hour pre-treatment, SDF-1 migration decreased significantly with 25mM extra glucose, showing that the addition of external glucose negatively affected migration. The application of sRAGE in the migration assay reversed the migration impairment for HL-60 cells. This phenomenon was further confirmed using primary mouse mononuclear blood cells. We determined that, while HL-60 migration was decreased in high glucose, cell viability, CXCR4 expression, and RAGE expression were consistent across HL-60 cell culture conditions. AGE content was significantly elevated for the HL-60 cells in the media condition with added glucose. The difference in migratory function was accounted for through the measurement of SDF-1 signaling. Whereas a spike of superoxide occurs

in response to SDF-1 added to cells in plain media, the starting baseline of superoxide is higher in cells cultured with added glucose, and the spike does not occur. Just as with migration, the application of sRAGE restored both the superoxide baseline and the spike of superoxide in response to SDF-1.

6.1.3 sRAGE Significantly Improves Wound Healing in a Diabetic Mouse Excisional Wound Model

We use a diabetic mouse excisional wound model to test the effectivenss of our treatments *in vivo*. We added buffer, SDF-1, sRAGE, and an sRAGE and SDF-1 combination as treatments within a dermal scaffold. When we originally compared free SDF-1 and buffer, we observed that SDF-1 did not improve healing compared to the buffer control. We then utilized sRAGE both alone and in combination with SDF-1, which we hypothesized would improve SDF-1 function. As previously seen in the literature, sRAGE significantly improved healing. However, while the sRAGE and SDF-1 combination did not significantly improve healing, it was slightly better than the free SDF-1. We therefore continued developing the SDF-1 delivery system for healing wounds by creating SDF-1 liposomes.

6.1.4 SDF-1 Liposomes Maintain SDF-1 Function In Vitro

After preparing SDF-1 liposomes consisting of negatively charged self-assembled liposomes and the positively charged SDF-1 molecule, we characterized them *in vitro* to see how well they maintain SDF-1 function. The formed SDF-1 liposomes retained 80% of the starting SDF-1 added to the mixture, indicating a high yield. To test for SDF-1 function, HL-60 cells were placed in the transwell migration assay and allowed to migrate to SDF-1 liposomes, which induced significant migration over the empty liposome and buffer controls, and, after 2 and 4 hours, was not significantly different from the free SDF-1. The SDF-1 liposomes also retained CXCR4 signaling; fluorescence microscopy was used to view the calcium response that occurs

when SDF-1 binds to the cell using a fluorescent calcium indicator. The calcium assay indicated there was no difference between SDF-1 liposomes and free SDF-1. In preparation for animal studies, the SDF-1 liposomes were placed in dermal scaffolds for delivery, where there was no hindrance to fast infiltration of the dermal scaffold by SDF-1 liposomes.

6.1.5 SDF-1 Liposomes Improve Wound Healing through Promotion of Proliferation and Wound Contraction.

The packaging of SDF-1 into liposomes had the most significant effect on healing, performing better than both free SDF-1, saline, and empty liposomes. Healing was more than 15% better than the other conditions at day 21, and it took the other groups about a week to catch up to the same level of healing. This difference in wound healing was due to sustained proliferation of cells in the dermis in SDF-1 liposome treated condition over the 28 day post-surgery period compared to the controls. While the histology suggests that the sustained proliferation is occurring in the endothelial cells, further staining will be used to confirm this hypothesis. The SDF-1 and SDF-1 liposome treated mice also had higher αSMA expression than the non-SDF-1 containing treatments, indicating that there was more wound contraction in the SDF-1 containing treatments.

6.2 LIMITATIONS

6.2.1 Choice of HL-60 Cells

One limitation of this dissertation is that most of the studies are done with the HL-60 cell line. HL-60 cells were chosen because they have a high expression of CXCR4 and act as a model cell line that experiences SDF-1 directed migration under normal conditions. Though they are distinct from the primary cells obtained from mouse blood, they are more practical to use as each mouse is limited to 1 mL per mouse cardiac puncture and the numerous *in vitro* studies would necessitate many mice. Also, the HL-

60 is a promyelocytic cell line, which is a mix of granulocyte precursors. This makes HL-60 cells an appropriate model, as well, because they represent inflammatory cells that would be implicated in the early stages of wound healing[1]. While the migration assay represents the action of SDF-1 on CXCR4 in inflammatory cells in the wound, endothelial cell and fibroblast responses may be different[2]; however differences can be observed in these HL-60s between normal and high glucose cultured cells. SDF-1 signaling responses observed through the calcium and superoxide assays have been previously observed in wound relevant cell types, such as hematopoietic stem cells[3] and endothelial progenitor cells[4], respectively.

6.2.2 Migration Assay

The transwell migration assay was selected based on its history of being a standard assay for measuring migration and use with the chemokine CXCR4 and HL-60 cells in prior literature. The transwell migration assay was the best choice for the HL-60 cells because they grow in suspension rather than attach to tissue culture plastic, so flat plane migration systems, where a horizontal gradient is setup, would not work. There are a few pitfalls to using the transwell migration assay. The chemokine solution on the bottom is separated by a thin porous membrane from the cells on top, so while there is an intial steep gradient, the top and bottom of the transwell equilibrate over time, making the gradient unstable. It's also not a high throughput system; in order to determine the number of cells that migrate through the membrane, the transwell membrane has to be removed. So, each well can only be used for one condition at one time-point. Migration from the same well cannot be tracked over time.

6.2.3 SDF-1

While the many positive attributes of SDF-1 have contributed to its selection, caution with SDF-1 must also be taken when translating SDF-1 from the benchtop to the clinic because of its implication in cancer. The discovery of SDF-1/CXCR4 signaling in

cells was first shown in chronic lymphocystic leukemia (CLL). Since then, the literature has shown that CXCR4 is upregulated in over 20 tumor types, plays a role in tumor metastasis via the migration and invasion of cancer stem cells (CSCs), and supports the survival and growth of fibroblasts in the tumor stroma[5]. Though many studies are currently investigating CSC stem cell properties and cell markers, being able to determine the effect of SDF-1 liposome wound treatment on CSC activity in animals could help determine safety of the treatment.

Another adverse effect of adding SDF-1 could be keloid development, though this is less likely in chronic wounds compared to acute wounds. In keloids, growth factors such as VEGF, transforming growth factor-β (TGF-β), and PDGF are overexpressed[6]. Because SDF-1 upregulates VEGF[7], there is a chance of an indirect effect on keloid formation; however, Regranex®, the only FDA-approved growth factor, is PDGF, and carries a similar risk.

Together with increasing the risk for cancer and scar formation, the packaging of SDF-1 and other growth factors for the clinic must be considered carefully. The liposomes increase availability and persistence of a growth factor, so dynamics can be explored *in vitro* and in preclinical animal studies to determine the growth factor concentration exposed to the tissue over time. It is possible that a one-time dose where growth factor is released over time will decrease the risk compared to multiple local applications of the free growth factors.

6.2.4 Liposome Formulation

When preparing the SDF-1 liposomes, we used only one formulation (10% negatively charged lipids, 20% cholesterol, 70% charged neutral lipids) in the studies. While the 10% negatively charged lipids must remain unchanged to balance the positively charged SDF-1, the fractions of cholesterol and neutral lipids can be modified. However, we did not modify them in these studies since our formulation produced a

functional SDF-1 liposome *in vitro* and an effective treatment *in vivo*. Because these studies were used to show SDF-1 effectiveness in wounds, we are still in the process of determining the mechanism behind their success *in vivo*. Once determining how they protect the SDF-1, future studies could determine if other lipid formulations produce a more stable and/or effective particle.

6.2.5 Excisional Wounding Studies

There were also limitations with the mouse wound model. Two different dermal scaffolds were utilized based on what was available for use. At certain points, either Alloderm® or Integra® was unavailable because the first priority is to get the product to the patients. This has limited the direct comparison between the sRAGE studies using Integra® and the SDF-1 liposome studies using Alloderm®. Also, the number of in vivo studies were limited due to the high cost of reagents and genetically modified animals, and this impacted the number of conditions tested and the number of animals per condition. Because of this limit, only one dosing combination of SDF-1 on day 0 and sRAGE on days 0, 2, 4, and 6 was utilized, leaving future studies to evaluate the timing of SDF-1 and sRAGE. We also noticed that the treatments more dramatically impacted the later stages of wound healing, as shown by the increased in cell proliferation and wound contraction. Therefore, future studies could utilize agents that provide a more significant effect at the earlier stages of wound healing. The mouse wounding model itself, while it's an in vivo representation of wound healing, also isn't a perfect representation of human wound healing. Humans heal primarily by reepithelialization and formation of granulation tissue; however, mice mainly heal by contraction. Also, mouse skin is more compliant than human skin and lacks sweat glands. Pig skin is a closer model to human skin than mice, but they incur higher costs and there are fewer reagents available for use in pigs[8].

6.3 FUTURE DIRECTIONS

Future studies include investigation of the mechanism of protection of SDF-1 by the liposomes in vivo. An interesting observation is that in vitro, free SDF-1 and liposomal SDF-1 behave very similarly. On the other hand, free SDF-1 had no effect in vivo, while liposomal SDF-1 improved wound healing rate. Through collaborating with Dr. Henry Hsia, we obtained wound fluid from patients with diabetes so that we can test how SDF-1 stability is affected by wound fluid and whether association with liposomal nanoparticles alters this stability. After determining how well the SDF-1 liposome protects the SDF-1 from degradation in wound fluid, further studies can be performed to determine the mechanism. For example, the liposomes could be acting by protecting SDF-1's binding site from being cleaved by proteases.

We also plan to combine both growth factor improvement strategies by combining the SDF-1 liposomes with sRAGE treatment. The combination can further be optimized by varying the timing and dose. Because the sRAGE acts on decreasing inflammation, it is possible that the most effective treatment strategy would be to first apply the sRAGE until the inflammatory phase has resolved into the proliferation phase. The SDF-1 liposomes could then be applied, since they improved cell proliferation and wound contraction, which are characteristics of the later stages of healing. This timing falls in line with SDF-1 production over the normal course of wound healing, which is increased at the wound margins day 7 post-wounding in mice[9] and days 10-21 post-wounding in humans[10] compared to immediately following wounding. It may be necessary to add subsequent doses of SDF-1 liposomes as well, though the goal is to get the greatest amount of effect with the least amount of drug applied.

The growth factor treatment improvement strategies used here could also be used as a platform to treat different wounds and beyond. For example, sRAGE treatment has the potential to improve other growth factors delivered to wounds and decrease MMP activity. The liposomes can be altered to be used with other peptides to treat

diabetic, biofilm-infected, and venous ulcers. These peptides can be small and positively charged already, or neutrally charged growth factors can be modified with a small positively charged peptide that would serve as a handle that would associate the growth factor with the negatively charged liposome.

In addition, these treatments can be combined with decellularized scaffolds to improve tissue regeneration in many different organs; they are currently used for skin bone[11] and are currently under development for complex organ regeneration such as the heart and liver[12-14]. The growth factor-associated liposome platform described here could then be easily incorporated into any of these scaffolds, since pore sizes are 2 orders of magnitude larger, around 10μm. While organ donations take place in a matter of hours, decellularized scaffolds have a long shelf-life. Therefore, the treatment outcome could then be scaffolds being thawed and loaded with agents that aid in tissue uptake and regeneration, such as growth factors loaded in nanoparticles and/or autologous or allogeneic cells.

6.4 REFERENCES

1 A. J. Almzaiel, R. Billington, G. Smerdon, and A. J. Moody, Effects of Hyperbaric Oxygen Treatment on Antimicrobial Function and Apoptosis of Differentiated Hl-60 (Neutrophil-Like) Cells, *Life Sci,* 93 (2013), 125-31.

2 B. A. Teicher, and S. P. Fricker, Cxcl12 (Sdf-1)/Cxcr4 Pathway in Cancer, *Clin Cancer Res,* 16 (2010), 2927-31.

3 A. Aiuti, I. J. Webb, C. Bleul, T. Springer, and J. C. Gutierrez-Ramos, The Chemokine Sdf-1 Is a Chemoattractant for Human Cd34+ Hematopoietic Progenitor Cells and Provides a New Mechanism to Explain the Mobilization of Cd34+ Progenitors to Peripheral Blood, *J Exp Med,* 185 (1997), 111-20.

4 D. J. Ceradini, D. Yao, R. H. Grogan, M. J. Callaghan, D. Edelstein, M. Brownlee, and G. C. Gurtner, Decreasing Intracellular Superoxide Corrects Defective Ischemia-Induced New Vessel Formation in Diabetic Mice, *J Biol Chem,* 283 (2008), 10930-8.

5 M. Cojoc, C. Peitzsch, F. Trautmann, L. Polishchuk, G. D. Telegeev, and A. Dubrovska, Emerging Targets in Cancer Management: Role of the Cxcl12/Cxcr4 Axis, *Onco Targets Ther,* 6 (2013), 1347-61.

6 D Robles, E Moore, M Draznin, and D Berg, Keloids: Pathophysiology and Management, *Dermatology Online Journal,* 13 (2007), 1-8.

7 J. Yamaguchi, K. F. Kusano, O. Masuo, A. Kawamoto, M. Silver, S. Murasawa, M. Bosch-Marce, H. Masuda, D. W. Losordo, J. M. Isner, and T. Asahara, Stromal Cell-Derived Factor-1 Effects on Ex Vivo Expanded Endothelial Progenitor Cell Recruitment for Ischemic Neovascularization, *Circulation,* 107 (2003), 1322-8.

8 V. W. Wong, M. Sorkin, J. P. Glotzbach, M. T. Longaker, and G. C. Gurtner, Surgical Approaches to Create Murine Models of Human Wound Healing, *J Biomed Biotechnol,* 2011 (2011), 969618.

9 T. E. Restivo, K. A. Mace, A. H. Harken, and D. M. Young, Application of the Chemokine Cxcl12 Expression Plasmid Restores Wound Healing to near Normal in a Diabetic Mouse Model, *J Trauma,* 69 (2010), 392-8.

10 A. Toksoy, V. Muller, R. Gillitzer, and M. Goebeler, Biphasic Expression of Stromal Cell-Derived Factor-1 During Human Wound Healing, *Br J Dermatol,* 157 (2007), 1148-54.

11 J. J. Song, and H. C. Ott, Organ Engineering Based on Decellularized Matrix Scaffolds, *Trends Mol Med,* 17 (2011), 424-32.

12 J. E. Arenas-Herrera, I. K. Ko, A. Atala, and J. J. Yoo, Decellularization for Whole Organ Bioengineering, *Biomed Mater,* 8 (2013), 014106.

13 A. Soto-Gutierrez, J. A. Wertheim, H. C. Ott, and T. W. Gilbert, Perspectives on Whole-Organ Assembly: Moving toward Transplantation on Demand, *J Clin Invest,* 122 (2012), 3817-23.

14 B. E. Uygun, M. L. Yarmush, and K. Uygun, Application of Whole-Organ Tissue Engineering in Hepatology, *Nat Rev Gastroenterol Hepatol,* 9 (2012), 738-44.